

Theoretical Study on the Potential Existing Forms and Microwave Rotational Spectrum of Short-Chain Fatty Acids in Interstellar Space

Fangjing Mu¹, Hao Wang², Zhanhang He³, Qian Gou^{2,*}, Yuchao Zhang^{4,*}, and Donghui Wei^{3,*}

¹ Academy for Advanced Interdisciplinary Studies (AAIS), Peking University, Beijing 100871, China.

² Green Catalysis Center, and College of Chemistry, Zhengzhou University, Zhengzhou, Henan 450001, China.

³ Department of Chemistry, School of Chemistry and Chemical Engineering, Chongqing University, Chongqing 401331, China

⁴ The Cancer Hospital of the University of Chinese Academy of Sciences, Institute of Basic Medicine and Cancer (IBMC), Chinese Academy of Sciences, Hangzhou, Zhejiang 310022, China

*Email: qian.gou@cqu.edu.cn (Qian Gou), yuchaozhang@ucas.ac.cn (Yuchao Zhang), donghuiwei@zzu.edu.cn (Donghui Wei)

Abstract

Several short-chain fatty acids and their corresponding potential existing hydrated forms are important molecules in interstellar space. Their structures were optimized with twelve different computational methods. The dipole moments and the spectral constants, including rotational constants and centrifugal distortion constants were obtained. According to the benchmark study, revDSD-PBEP86-D3(BJ) is the most suitable method that was selected for rotational calculation. Symmetry-adapted perturbation theory was used to study the strength and composition of the interaction between acids and water in clusters. The possibility of its existing under the low-temperature and low-pressure conditions was confirmed by calculating of binding free energy. Furthermore, *ab initio* molecular dynamics simulations were used to investigate whether the internal rotations of acids could be observed. The 3-fold splitting from the predicted high-resolution microwave rotational spectra of the acetic acid monohydrate at different temperatures perfectly proved the accuracy of the simulations.

Keywords: Short-chain fatty acids; Microwave rotational spectroscopy; Interstellar molecules; *Ab initio* molecular dynamics simulation; Energy decomposition analysis.

1. Introduction

Microwave Rotational Spectra are used to not only diagnose the physical state of molecules in circumstellar nebulae and envelopes., but also confirm the molecules in interstellar space, then the abundance of molecules can be reflected by strength of spectra, thus indicating the temperature of the environment. Derived from this, organic molecules such as formic acid and acetic acid have been widely observed in space by assistance of its microwave rotational spectrum¹. Short-chain fatty acids (SCFAs), also known as volatile fatty acids, usually refer to saturated fatty acids with 1 to 6 carbon atoms. Apart from being observed by telescope, they have also been found in meteorites. Propionic acid is the most abundant monocarboxylic-acid-type soluble organic matter in Murchison meteorites²⁻⁴. Generally, fatty acids play a pivotal role in the origin of life because SCFAs and their hydrates are

the basis for the existence of carbon-based life. SCFAs are precursor molecules of life and form the basis for the existence of carbon-based life, and have significant biological significance. It's putative that fatty acids form biological membranes by combining with glycerol and phosphoric acid to form phospholipids. Noteworthy, fatty acid membranes bind to amino acids, which can stabilize biomembranes and they can contribute to the eventual formation of proteins⁵. In addition, SCFAs are the main metabolic products by microbiota⁶, in which case, they play an important role in physiological and biochemical processes⁷. Consequently, it is possible to study the composition of the upper atmosphere of a planet by studying the microwave spectral satellite lines of organic acids and their water clusters, and then to search for life matter and explore whether extraterrestrial life exists in the vast universe.

Recently, tremendous advances have been achieved in the study of microwave rotational spectroscopy of small organic molecules. The widely use of Fourier transform microwave spectrometer provide great convenient to scientists to obtained multifarious rotational spectra of organic molecules on the earth, and extracted more accurate structure information. In order to investigate the configuration of SCFAs hydrate clusters, the Howard group studied the microwave spectra of propionic acid (PPA) and its hydrates by configuring solutions with different ratios in 2008, obtaining information such as molecular structure, spectroscopic constants, and binding energy⁸. Similarly, in 2009, the group studied the microwave spectra of acetic acid (AA) and its hydrate clusters⁹, and it can be inferred that SCFAs hydrate clusters may exist in the form of monohydrates and dihydrides in interstellar space. Weak interactions exist in hydrate clusters, and in experiments, conformational analysis and hydrogen bond parameters can be studied by analyzing the microwave rotational spectra¹⁰. In 2017, Caminati and his coauthors analyzed the rotation of acetic acid and fluorinated acetic acid dimers, revealing the role of hydrogen bonding between organic acids¹¹. Additionally, Internal rotation in interstellar molecules is an important research topic in astrochemistry. Experimental scientists can observe the microwave rotational spectra of small molecules using instruments such as FTMW, and then analyze internal rotation and other large-amplitude motions through spectral line splitting. In 2011, Caminati's research group studied the rotational spectra of 2-butyric acid, mainly exploring internal rotation issues¹². In 2017, the group analyzed the rotational motion of acetic acid and fluorinated acetic acid dimers¹³. To the best of our knowledge, systematic theoretical computational studies on the microwave rotational spectroscopic properties of common volatile SCFAs and their hydrated clusters lag behind.

In this work, we aim to simulate straight SCFAs (Ac) and their hydrate clusters, namely acetic acid (AA), propionic acid (PPA), butyric acid (BA), pentanoic acid (PTA), hexanoic acid (HXA) and their monohydrate clusters (Ac-w) and dihydrate clusters (Ac-w₂). We only consider mono- and dihydrates because the collision and combination probability of SCFAs with three or more molecules of water has already been relatively low. Systematic calculations were performed on them using *ab initio* and DFT methods. Information like geometric structures, rotational constants (*A*, *B*, *C*), centrifugal distortion constants (Δ_J , Δ_K , Δ_{JK} , δ_J , δ_K), molecular electric dipole moments, and components in orthogonal directions ($|\mu_{TOT}|$, $|\mu_a|$, $|\mu_b|$, $|\mu_c|$), isomerization transition state and corresponding Gibbs free energy barrier (ΔG^\ddagger) of internal rotations can be obtained. It should be mentioned that the most suitable calculation method for such system was confirmed after being compared with the existing experimental results. Additionally, the composition of dissociation energy (ΔG) was studied and the

internal rotation and cluster stability were simultaneously studied using *ab initio* molecular dynamics (AIMD) innovatively at different temperatures. These results will provide new insights for the development of molecular spectroscopy and its application in the chemistry field.

2. Computational details

In the very first place, we constructed structural models of AA, PPA, BA, PTA, HXA and their mono- and dihydrates, and performed the completely geometric optimization using the Gaussian16 package¹⁴. Applied with Grimme's D3 correction¹⁵ with Becke-Johnson (BJ)¹⁶, we used Generalized Gradient Approximation (GGA) BLYP-D3(BJ)¹⁷⁻¹⁹, meta-Generalized Gradient Approximation (meta-GGA) MN15L-D3^{20,21}, Hybrid GGAs B3LYP-D3(BJ)²²⁻²⁴, PBE0-D3(BJ)²⁵⁻²⁷ and ω B97X-D²⁸, Hybrid meta-GGAs M06-2X(D3)^{29,30} and MN15-D3(BJ)^{21,31}, Double Hybrid Density Functionals (DHDFs) B2PLYP-D3(BJ)^{32,33}, spin-scaling DHDFs DSD-PBEP86-D3(BJ)³⁴ and revDSD-PBEP86-D3(BJ)³⁵, and wave function (WF) based methods HF and MP2, which are combined with basis set may-cc-pVTZ³⁶⁻³⁸ for all atoms, respectively. The optimized structures were confirmed to be minimum points by frequency analyses, and the Cartesian coordinates were given in **Supporting Information**. Since they are all asymmetric-top molecules, the dipole moment obtained by structural optimization can determine the type of rotational spectra. In addition, the centrifugal distortion constants were acquired by calculating the resonant frequency of the vibration-rotation coupling. Compared with the calculated rotational constants of AA, PPA and their hydrates with the experimental values^{8,9}, the optimal calculation method for this kind of system was identified. Furthermore, the Root Mean Square Difference (RMSD) was calculated based on the geometric optimization results, and different methods were evaluated to reflect the reliability of optimizing the structures.

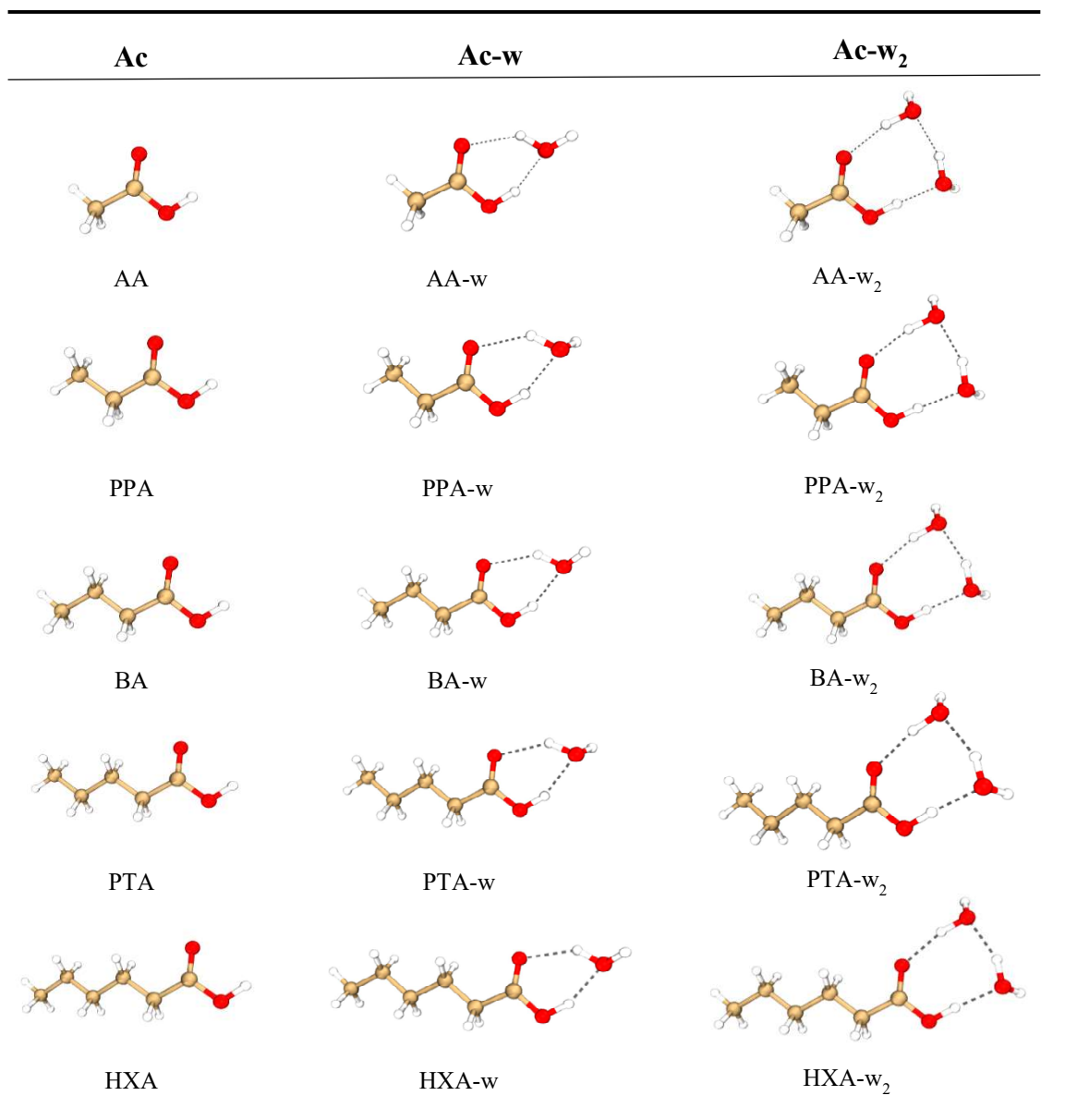
Applying high order symmetry-adapted perturbation theory (SAPT)³⁹, we used the PSI4 1.5⁴⁰ program to perform the energy decomposition calculation for the weak interaction in the SCFA hydrates model at the gold standard^{41,42} of SAPT2+(3) δ MP2/aug-cc-pVTZ^{38,43-45} with unfrozen nucleus, and the total interaction energy and its four energy components were obtained. Moreover, the dissociation Gibbs free energies at different temperatures were corrected using Shermo 2.3⁴⁶ software from the results above. Including dispersion interactions, we employed the revDSD-PBEP86-D3(BJ) functional combined with may-cc-pVTZ basis set to scan the rotation of terminal methyl dihedral (Φ), and then located the rotation transition state and calculated the V_3 energy barrier for terminal methyl rotation. Ultimately, we performed AIMD studies derived from adiabatic approximation for acetic acid monohydrate (AA-w), butyric acid (BA-w), and (HXA-w) using ORCA 5.0.2 program^{47,48} with PBE0-D3(BJ)/def2-TZVP⁴⁹, and further got the stability and vibration characteristics of the clusters within 1 ps time scale at 5 K, 50 K, and 100 K, separately. Meanwhile, Rijcosx algorithm⁵⁰ was used to accelerate the calculation by reducing the time-consuming calculation of hybrid functionals dramatically. Predicted high resolution microwave rotational spectra were used to study gaseous molecules in isolated systems under vacuum, and they were obtained from Herb Pickett's SPCAT program⁵¹. All of the structures were visualized by Visual Molecular Dynamics (VMD) software⁵² and the microwave spectra were visualized by pgopher⁵³.

3. Results and discussion

3.1 Optimized structures

Inspired by the conformations of AA hydrates⁵⁴, we have constructed a series of initial structures of Ac, Ac-w and Ac-w₂. We have optimized structures of the various acids Ac and the corresponding water clusters Ac-w and Ac-w₂ at the twelve computational levels, and those structures optimized at the revDSD-PBEP86-D3(BJ)/may-cc-pVTZ level have been summarized in **Table 1**. From the average of the RMSD values provided in **Table S1** of **SI**, the differences between the geometrical structures are tiny, indicating the optimized structures are reliable.

Table 1 The optimized structures of the Ac and the corresponding Ac-w and Ac-w₂ at the revDSD-PBEP86-D3(BJ)/may-cc-pVTZ level



On the basis of the optimized structure, the same level calculations were performed to obtain the microwave rotational spectral constants, including the rotational constants and centrifugal distortion

constants, for all the Ac, Ac-w, Ac-w₂ by using different methods, which can be found in **Table 2** and **Tables S2.1-2.14 of Supporting Information (SI)**. Our calculation results of AA and PPA summarized in **SI** are similar to those reported by Howard and Stiefvater et al. before^{8,9,55}, indicating that calculation results are reasonable and reliable.

Table 2 Rotational constants, centrifugal distortion constants, and dipole moment of PTA-w calculated by using the twelve different methods

PTA-w	B2PLYP-D3(BJ)	B3LYP-D3(BJ)	BLYP-D3(BJ)	DSD-PBEP86-D3(BJ)	HF	M06-2X(D3)	MN15-D3(BJ)	MN15L(D3)	MP2	PBE0-D3(BJ)	revDSD-PBEP86-D3(BJ)	ω B97X-D
<i>A</i> (MHz)	6265.7469	6282.6554	6178.8430	6251.2776	6354.6294	6258.7835	6232.8379	6075.0504	6244.8708	6338.1422	6243.7290	6317.8185
<i>B</i> (MHz)	636.9897	635.2661	625.9084	638.9130	617.2387	639.6434	641.3249	620.6068	640.9577	644.3143	636.3199	635.6219
<i>C</i> (MHz)	587.1183	585.8340	577.1507	588.6847	570.7288	589.2361	590.4707	571.6824	590.3146	594.0652	586.4236	586.4691
Δ_J (kHz)	31.024	30.376	30.265	31.434	36.772	31.479	33.223	34.322	32.310	31.116	31.744	30.728
Δ_K (kHz)	20151.556	20008.733	19238.550	20091.078	31624.769	21159.931	21202.182	24202.347	20200.441	19520.362	20509.788	19913.362
Δ_{JK} (kHz)	-608.438	-597.478	-564.093	-615.926	-801.235	-617.467	-661.344	-631.358	-623.002	-617.499	-626.043	-617.799
δ_J (kHz)	4.191	4.087	4.024	4.262	4.839	4.300	4.588	4.555	4.371	4.223	4.296	4.135
δ_K (kHz)	-48.252	-19.301	-105.699	-25.123	93.813	36.675	62.739	96.278	-93.955	-14.335	-14.462	-36.573
$ \mu_a $ (D)	0.55	0.62	0.72	0.52	0.32	0.43	0.45	0.28	0.47	0.62	0.50	0.59
$ \mu_b $ (D)	0.20	0.29	0.31	0.19	0.15	0.14	0.20	0.22	0.10	0.33	0.18	0.32
$ \mu_c $ (D)	1.22	1.24	1.26	1.23	1.02	1.16	1.19	1.15	1.20	1.27	1.22	1.26
$ \mu_{tot} $ (D)	1.35	1.41	1.49	1.34	1.08	1.24	1.29	1.20	1.29	1.45	1.33	1.43

Based on the optimized structures and microwave rotational constants *A*, *B*, and *C*, we further investigated whether Ac, Ac-w, and Ac-w₂ have rotational transitions. As we all know, a asymmetric molecule with *A*>*B*>*C* interacts appreciably with a microwave electromagnetic field to emit or absorb radiation only if it has an electric or magnetic dipole moment⁵⁶, and a non-zero dipole moment component in *x*, *y*, or *z* direction, which means that there can be corresponding *a*-, *b*- or *c*-type of transition. It is reported that revDSD-PBEP86-D3(BJ) is suitable to calculate the electron structures³⁵, so it can be good at calculating dipole moments. Due to the fact that the $|\mu_a|$, $|\mu_b|$, and $|\mu_{tot}|$ calculated with revDSD-PBEP86-D3(BJ)/may-cc-pVTZ can basically match with the experimental data^{9,55}, so these data are mainly regarded as the prediction of dipole moment. For the SCFAs, they are all asymmetric-top molecules but the nearly symmetric planar, which causes the absence of *c*-dipole moment, indicating that the *c*-type transition cannot occur. Take AA as an example, after calculation, its *A*, *B*, *C* constants are decreasing (11327.7036, 9492.0740, 5334.6625), so AA is an asymmetric-top molecule. and the $|\mu_a|$, $|\mu_b|$, and $|\mu_c|$ of it is in turn 0.86, 1.47, and 0.00 (**SI Table S1.1**), so it may have *a*- and *b*-type spectra and definitely cannot have a *c*-type spectrum. Like PTA-w, $|\mu_a|$, $|\mu_b|$, and $|\mu_c|$ selection rules are active, so three types of transitions may occur (the dipole moment data were summarized in **Table 2**). However, according to previous reports^{9,57}, tunnel effect can occur for the motions of uncoordinated H atoms, so some *c*-type spectra may not be observed in the clusters Ac-w and Ac-w₂.

3.2 Benchmark of rotational constants

To test the reliability of the selected twelve computational method, we compared the calculated data with the experimental data^{8,9}. Due to the fact that the molecules mainly rotate in the ground state at

low temperature and low pressure, the rotation constants A , B and C are enormously more important in the microwave rotational spectra, in which case we need to find the most suitable method for calculating A , B and C . As shown in **Fig. 1**, the absolute errors (AE) from the six experimental reference values^{8,9} of A for AA, PPA and their corresponding hydrates and the correspondingly calculated data obtained by the twelve methods were set as the vertical axis. Moreover, we have performed linear regression for them to get the slope, intercept, and squared residual (R^2), mean absolute deviations (MADs) of slope and intercept, which were summarized in **Table S3 of SI**.

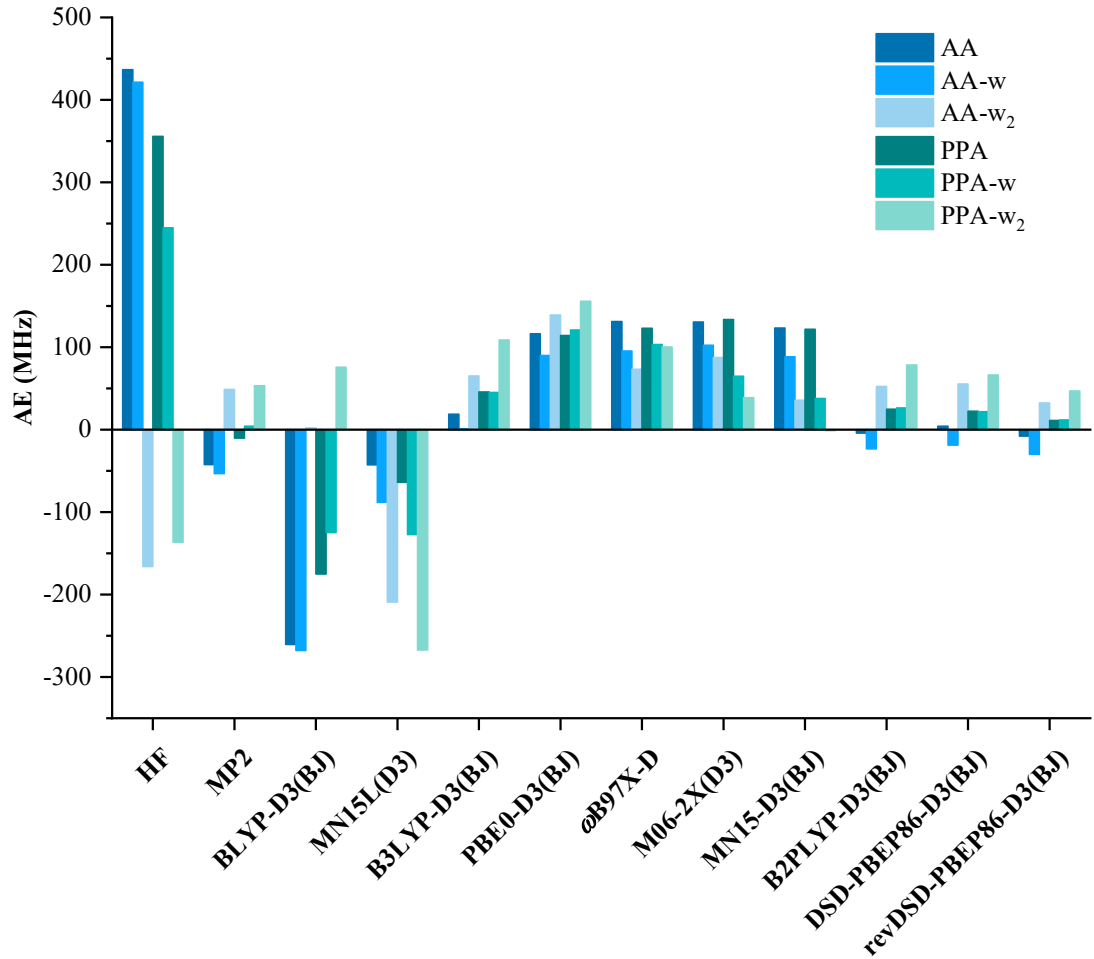


Fig. 1 The AE for rotational constant A of AA, AA-w, AA-w₂, PPA, PPA-w, and PPA-w₂ by using twelve methods (may-cc-pVTZ basis set)

With the lower MADs and the closer slopes to 1, the DHDFs are the most suitable methods for the calculation of rotational constants for SCFAs and their hydrates, and the performance of revDSD-PBEP86-D3(BJ) with the slope of 0.99903 is the best one. Among the hybrid functionals, PBE0-D3(BJ), B3LYP-D3(BJ) and ω B97X-D perform better than the other functionals. Furthermore, the linear regression result obtained by the HF method deviates the most. Although the MP2 method also has the good performance as the hybrid GGA functional, it has consumed relative long time.

The computational time of MP2 approximately equals to that of hybrid functional methods. For example, using HXA-w₂ as an example, the CPU running time for geometry optimization at the revDSD-PBEP86-D3(BJ)/may-cc-pVTZ level is 2 days and 20 hours, while the same basis set with MP2 method requires 3 days and 6 hours, making the MP2 method less cost-effective.

In addition, some studies advocate using the MP2 method for geometry optimization and then performing single-point correction to MP2 energy calculations using the CCSD(T) method ($\text{MP2} + \Delta\text{CCSD(T)}$) to study interstellar molecular structures, molecular spectroscopic constants, and molecular energies⁵⁸. Through the testing and discussion above, it was found that the revDSD-PBEP86-D3(BJ) method, which is comparable to the MP2 on structure optimization in terms of time, has advantages in optimizing structures and calculating rotational constants. Although the CCSD(T) method is more accurate than rev-DSD-PBEP86-D3(BJ) in calculating electronic energy, it cannot obtain information such as free energy correction quantities without the Hessian matrix for vibrational analysis in software such as *Gaussian*. Even if computable software is used, the required time is longer. This combined method is inferior to the rev-DSD-PBEP86-D3(BJ) method in terms of calculating electronic structure, electron density, dipole moment, rotational constants, thermodynamic energy, and computational time.

3.3 Stability of the clusters

Aimed at exploring whether the rotation of the Ac-w and Ac-w₂ in the vibrational ground state can still maintain the cluster morphology at low temperature and low pressure, we constructed four water-losing models: (i) the monohydrate loses one molecule of water, (ii) the water dimer loses two molecules of water, (iii) the water dimer loses one molecule of water, (iv) the water dimer loses another molecule of water. To study the strength and the composition of the hydrogen bonds, we did the SAPT energy decomposition calculation for the hydrated cluster, and decomposed the energy of hydrogen bond between molecules into electrostatic interactions, exchange mutual repulsion, induction, and dispersion. As can be seen from **Fig. 2**, the electrostatic attraction with positive contribution dominates in the hydrated clusters, whilst the dispersion and induction play an auxiliary role. The exact data for electrostatics, exchange, induction, dispersion and total SAPT2+(3) δMP2 energy is summarized in **Table S4**. In addition, according to the total SAPT2+(3) δMP2 in the figure, the decomposition of water dimer requires more energy to lose two water molecules, so the dimer is more stable. Furthermore, it can be known from **Table 2** and **Table S2.1-2.14** in **SI** that water restricts the rotation of the acid. That is to say, we can see that the more the coordination is corresponding to the smaller the rotational constant and the smaller the moment of inertia, so it is easier to rotate in the ground state, and the energy is lower. In conclusion, the SCFAs in the outer space will preferentially form more stable dihydrate clusters.

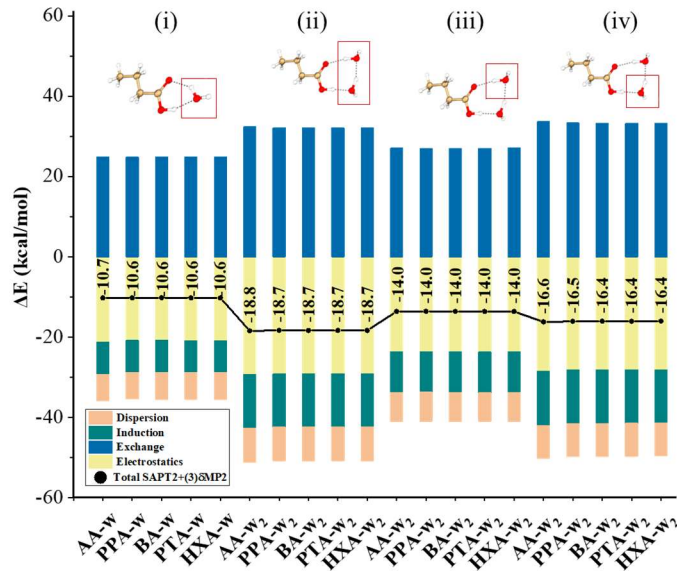


Fig. 2 Decomposition energy diagram of hydrogen bonds in four types of clusters using SAPT

In order to explore whether such cluster structures can be maintained during rotation at different temperatures in the presence of water, both the stability of the two kinds of hydrates were investigated as follows. As we all know, SAPT only computes the electronic energy without the thermal corrections, here we further calculated the Gibbs free energies with the thermal corrections at different temperatures and the values are provided in **Table S5**. After that, ΔG of the dehydration procedure of water monomer and water dimer can be calculated (**Table S6**). It is found that the ΔG decreases with the rise of temperature so the stability declines.

Taking Gibbs-Helmholtz equation into the consideration, we set $\lg(\text{reactant}/\text{product})$ as the ordinate, and its change with temperature is shown in **Fig. 3**. At 200 K and below, the ratio of the reactant (i.e. monohydrate or dihydrate cluster) to the product loses a molecule of water is greater than 1000:1, which indicates a great advantage in the form of clusters. In other words, rotation at higher temperatures than 200 K may lead to changes in the cluster skeleton.

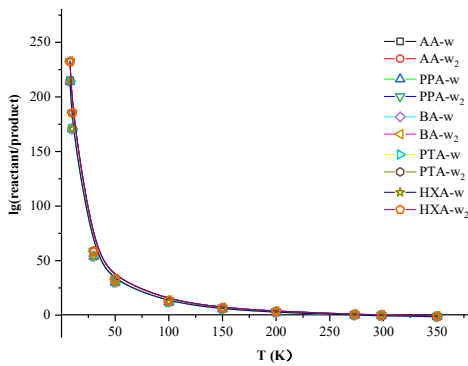


Fig. 3 The relationship between the ratio of clusters and dehydrated molecules at different temperatures

3.4 Internal rotation

In order to explore whether the internal rotation of different acids occurs in the microwave rotation

spectrum at low temperature and low pressure, we performed an energy surface scan on the Φ of the terminal methyl group to get V_3 barrier. The electron energy difference ΔE^\ddagger between the eclipsed and staggered conformation is shown in **Table 4**. We can see that ΔE^\ddagger is high, so when the rotor is regarded as a rigid rotor, the spectrum will not split without internal rotation at low temperature, theoretically. To explore the relationship between internal rotation and temperature, we located the rotational transition state (**SI**) and added the thermo corrections to the acids and clusters at 5 K, 50 K, 100 K and 298 K, which are shown in **Table 4** as well. Accompanied with the increasing temperature, the ΔG^\ddagger becomes larger, possibly enabling the methyl group to overcome the rotational energy barrier. It can be seen that the barriers for SCFAs and clusters containing three carbons and more are relatively high, we deduce that internal rotations for them cannot occur. But it cannot be confirmed that whether rotation of $-\text{CH}_3$ can occur in real situations, especially for AA and its clusters merely with the data of ΔE^\ddagger and ΔG^\ddagger .

Table 4 Internal rotational electronic energy barrier ΔE^\ddagger and the rotational Gibbs free energy barrier ΔG^\ddagger calculated at the level of revDSD-PBEP86-D3(BJ)/may-cc-pVTZ at different temperatures.

	ΔE^\ddagger (kJ/mol)	ΔG^\ddagger (5 K, kJ/mol)	ΔG^\ddagger (50 K, kJ/mol)	ΔG^\ddagger (100 K, kJ/mol)	ΔG^\ddagger (298 K, kJ/mol)
AA	1.64	1.51	1.58	1.92	4.74
AA-w	1.34	1.22	1.32	1.72	4.83
AA-w ₂	1.12	1.03	1.16	1.63	5.02
PPA	10.10	9.35	9.37	9.48	10.91
PPA-w	10.22	9.41	9.43	9.53	10.88
PPA-w ₂	10.35	9.56	9.58	9.68	11.03
BA	12.96	12.19	12.20	12.26	13.38
BA-w	12.98	12.19	12.20	12.25	13.31
BA-w ₂	12.98	12.20	12.20	12.26	13.32
PTA	12.39	11.62	11.63	11.69	12.83
PTA-w	12.39	11.63	11.64	11.70	12.88
PTA-w ₂	12.39	11.61	11.61	11.67	12.79
HXA	12.40	11.62	11.63	11.68	12.78
HXA-w	12.39	11.62	11.63	11.70	12.85
HXA-w ₂	12.39	11.61	11.62	11.68	12.81

3.5 AIMD simulations

Considering the representativity and comparability, we selected the moderate SCFA monohydrates with even number of carbons (**Fig.4**) to study the dynamic behavior in real situations.

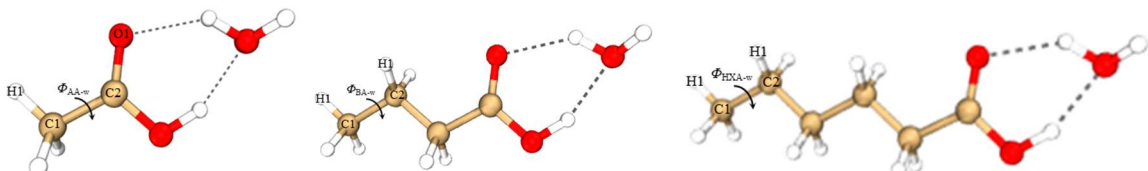


Fig. 4 The structures and investigated dihedral angels of AA-w, BA-w and HXA-w

According to molecular dynamics we further verified whether the clusters are stable and whether internal rotations can occur at the temperatures of 5 K, 50 K, and 100 K. Atomic velocities were randomly initialized by Maxwell distribution AIMD simulations of 10 ps were performed at the PBE0(D3)/def2-TZVP level using a canonical sampling through velocity rescaling (CSVR) thermostat. The dihedral angle of terminal $-\text{CH}_3$ Φ is mainly investigated. Taking BA-w at 5 K as an example, we procured the trajectory based on AIMD, which is shown in **Fig. 4**. At this time scale, the dihedral angle

$\Phi_{\text{BA-w}}$ is twisted between 54.67° and 62.03° and the optimized dihedral angle is 58.20° , in which case, BA-w only performs small-scale thermal fluctuations in stable conformational space and there is no internal rotation at 5 K.

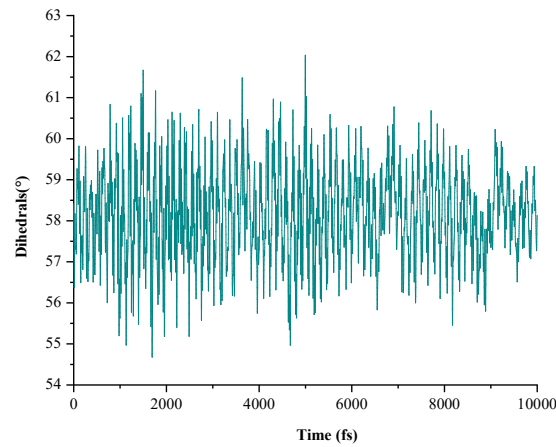
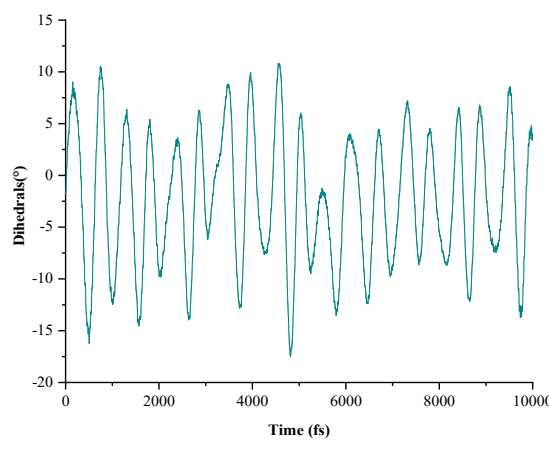


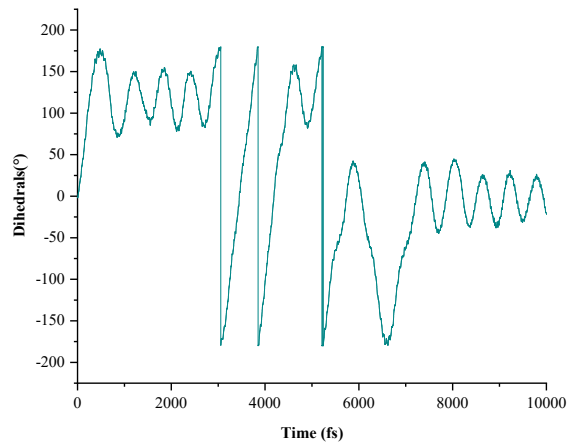
Fig. 5 The change of $\Phi_{\text{BA-w}}$ in 10 ps (5 K)

At 5 K, we also provided the change of $\Phi_{\text{AA-w}}$ in **Fig. 6 (a)** and $\Phi_{\text{HXA-w}}$ in SI (**Fig. S3.1**). Both of the rotations of the methyl are small and cannot cause the spectral splitting. According to **Fig. 5**, **Fig. 6 (a)**, and **Fig. S3.1**, there are small differences for the dihedral angle, indicating the SCFAs can exist stably. Due to the fact that the experimental conditions of microwave spectroscopy are extremely low temperature (<10 K) in order to simulate the interstellar space, internal rotation cannot occur and no 3-fold splitting can be observed.

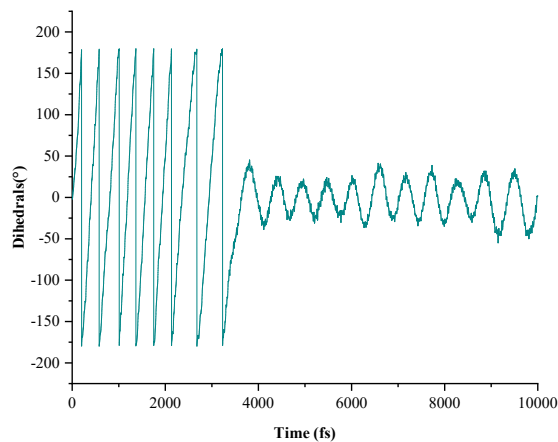
Then we explored the internal rotation of the methyl group with the rise of temperature. According to the optimized structure, the $\Phi_{\text{AA-w}}$ is -1.78° . At 5 K, it swings at a relatively small scale from -17.51° to 10.82° (**Fig. 6a**), it will not cross the internal rotation energy barrier. Nonetheless, internal rotation can occur at both 50 K and 100 K and AA-w rotate more freely at 100 K (**Fig. 6b, c**).



(a)



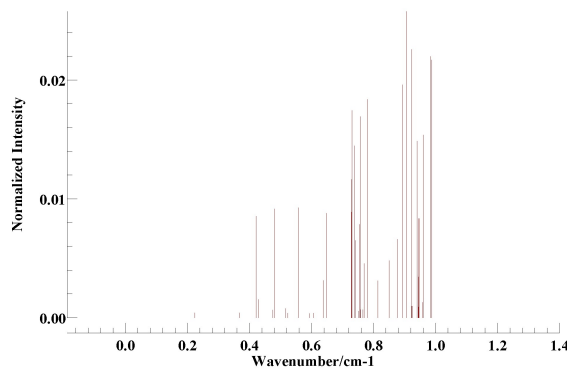
(b)



(c)

Fig. 6 (a), (b), (c) The change of Φ_{AA-w} in 10 ps at 5 K, 50 K and 100 K

Applied with SPCAT, we used the experimental data⁹ to predict the microwave rotational spectroscopy. The spectral line files of the AA-w molecules were visualized with pgopher and shown in **Fig. 7 (a), (b), (c)**. It can be seen that the spectra unsplit at 5 K, and split at 50 K and 100 K. The corresponding methyl group does not rotate at 5 K, but rotates at 50 K and 100 K, and the figure is consistent with the results obtained by AIMD (**Fig. 6 (a), (b), (c)**).



(a)

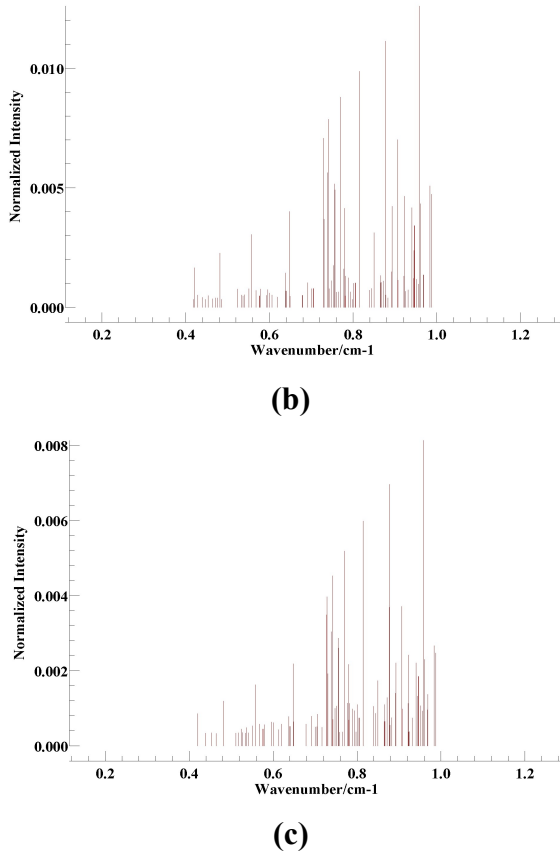


Fig. 7 (a), (b), (c) Microwave rotational spectra of AA-w at 5 K, 50 K and 100 K

However, in **Fig. S3.2-3.5**, we provided the dihedral rotation angle of the 10 ps AIMD simulation of BA-w and HXA-w at 50 K and 100 K, and the change of Φ were both small and no internal rotation occurred, which can perfectly correspond to the conclusion based on energy barrier.

In order to investigate why only AA-w can rotate at high temperature, we further compared the structure of AA-w and BA-w for the difference of the rotation of Φ in **Fig.8**. For the van der Waals radius of H, O atoms are 1.0 Å and 1.35 Å, the minimum distance that atoms can interact with each other are $r_{\min}(H \dots H) = 2.0 \text{ \AA}$ and $r_{\min}(H \dots O) = 2.5 \text{ \AA}$, respectively⁵⁹. For AA-w, the distance $r(H \dots O)$ of H1 and O1 is 2.6 Å when Φ equals to zero, so the methyl can rotate with sufficient energy provided by temperature. However, $r(H \dots H)$ of BA-w is 2.3 Å, lower than 2.5 Å, which means van der Waals interaction exists.

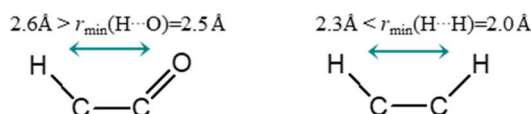


Fig.8 The contracts of the intramolecular interaction of H atom from terminal -CH₃ and O or H atom on adjacent carbon for AA-w and BA-w

It can be concluded that the presence of the methylene group hinders the rotation of the terminal methyl group.

4. Conclusion

The geometries of SCFAs have been optimized using twelve computational methods, respectively, which provide rotational spectroscopic parameters (rotational and centrifugal distortion constants) of target molecules, directly reflected by their mass distribution. Taken experimental values of rotational spectroscopic parameters by high resolution rotational spectroscopy as the benchmark, the revDSD-PBEP86-D3(BJ) was determined to be the optimal calculation method, and the DHDFs have excellent performance. When the computing resources are limited, PBE0, B3LYP, and ω B97X-D can be selected for ordinary functionals to calculate the rotational spectra of such substances.

The geometries of SCFAs have been optimized using twelve computational methods, respectively, which provide rotational spectroscopic parameters (rotational and centrifugal distortion constants) of target molecules, directly reflected by their mass distribution. Taken experimental values of rotational spectroscopic parameters by high resolution rotational spectroscopy as the benchmark, the revDSD-PBEP86-D3(BJ) was determined to be the optimal calculation method, and the DHDFs have excellent performance. When the computing resources are limited, PBE0, B3LYP, and ω B97X-D can be selected for ordinary functionals to calculate the rotational spectra of such substances.

The decomposing energy of SCFA...water bonds in the hydrated clusters indicated that the electrostatic attraction was dominant in the hydrated clusters, and there were also dispersion and dissociation effects. By analyzing rotation constants, it is known that SCFAs in space will preferentially form more stable dihydrate clusters. In addition, by penetrating into the water loss reaction process, it is known that the critical temperature for maintaining the hydrated cluster structure is approximately equal to 200 K.

Through analyzing ΔG^\ddagger and ΔE^\ddagger from potential energy surface scanning and transition state optimization, the possibility of internal rotation can be conjecture. According to AIMD simulations, the real dynamic change of the dihedral angle of the terminal methyl group provides theoretical support for whether three-fold splitting occurs due to internal rotation, and innovatively opens up new ideas for predicting splitting. In conclusion, SCFAs exist stably at 5 K to 100 K and Φ s of SCFAs do not undergo internal rotation at 5 K. Φ_{AA-w} rotates at 50 K and above, but for SCFAs with three or more carbons, the methyl groups are difficult to rotate even at 100 K. We verified the existence of methylene group hinders the rotation of the terminal methyl group.

In addition, the parameter data that have not been reported experimentally can be used as the theoretical prediction result, because the computational accuracy was tested to be high enough.

References

1. Solomon, P. M. Interstellar molecules. *Phys. Today* **26**, 32–40 (1973).
2. Kitadai, N. & Maruyama, S. Origins of building blocks of life: A review. *Geosci. Front.* **9**, 1117–1153 (2018).
3. Sephton, M. A. Organic compounds in carbonaceous meteorites. *Nat. Prod. Rep.* **19**, 292–311 (2002).
4. Lawless, J. G. & Yuen, G. U. Quantification of monocarboxylic acids in the Murchison carbonaceous meteorite. *Nature* **282**, 396–398 (1979).

5. Cornell, C. E. *et al.* Prebiotic amino acids bind to and stabilize prebiotic fatty acid membranes. *Proc. Natl. Acad. Sci.* **116**, 17239–17244 (2019).
6. Frampton, J., Murphy, K. G., Frost, G. & Chambers, E. S. Short-chain fatty acids as potential regulators of skeletal muscle metabolism and function. *Nat. Metab.* **2**, 840–848 (2020).
7. Canfora, E. E., Jocken, J. W. & Blaak, E. E. Short-chain fatty acids in control of body weight and insulin sensitivity. *Nat. Rev. Endocrinol.* **11**, 577–591 (2015).
8. Ouyang, B. & Howard, B. J. High-Resolution Microwave Spectroscopic and ab initio Studies of Propanoic Acid and Its Hydrates. *J. Phys. Chem. A* **112**, 8208–8214 (2008).
9. Ouyang, B. & Howard, B. J. The monohydrate and dihydrate of acetic acid: A high-resolution microwave spectroscopic study. *Phys Chem Chem Phys* **11**, 366–373 (2009).
10. Su, Z., Wen, Q. & Xu, Y. Conformational Stability of the Propylene Oxide–Water Adduct: Direct Spectroscopic Detection of O–H···O Hydrogen Bonded Conformers. *J. Am. Chem. Soc.* **128**, 6755–6760 (2006).
11. Feng, G., Gou, Q., Evangelisti, L. & Caminati, W. Rotational study of the bimolecule acetic acid-fluoroacetic acid. *Chem. Phys. Lett.* **667**, 154–157 (2017).
12. Ilyushin, V. *et al.* Almost free methyl top internal rotation: Rotational spectrum of 2-butynoic acid. *J. Mol. Spectrosc.* **267**, 186–190 (2011).
13. Feng, G., Gou, Q., Evangelisti, L. & Caminati, W. Rotational study of the bimolecule acetic acid-fluoroacetic acid. *Chem. Phys. Lett.* **667**, 154–157 (2017).
14. Frisch, M. J. *et al.* Gaussian 16 Rev. C.01. (2016).
15. Grimme, S., Antony, J., Ehrlich, S. & Krieg, H. A consistent and accurate *ab initio* parametrization of density functional dispersion correction (DFT-D) for the 94 elements H–Pu. *J. Chem. Phys.* **132**, 154104 (2010).
16. Grimme, S., Ehrlich, S. & Goerigk, L. Effect of the damping function in dispersion corrected density functional theory. *J. Comput. Chem.* **32**, 1456–1465 (2011).
17. Becke, A. D. Density-functional exchange-energy approximation with correct asymptotic behavior. *Phys. Rev. A* **38**, 3098–3100 (1988).
18. Lee, C., Yang, W. & Parr, R. G. Development of the Colle-Salvetti correlation-energy formula into a functional of the electron density. *Phys. Rev. B* **37**, 785–789 (1988).
19. Miehlich, B., Savin, A., Stoll, H. & Preuss, H. Results obtained with the correlation energy density functionals of becke and Lee, Yang and Parr. *Chem. Phys. Lett.* **157**, 200–206 (1989).
20. Yu, H. S., He, X. & Truhlar, D. G. MN15-L: A New Local Exchange-Correlation Functional for Kohn–Sham Density Functional Theory with Broad Accuracy for Atoms, Molecules, and Solids. *J. Chem. Theory Comput.* **12**, 1280–1293 (2016).
21. Goerigk, L. *et al.* A look at the density functional theory zoo with the advanced GMTKN55 database for general main group thermochemistry, kinetics and noncovalent interactions. *Phys. Chem. Chem. Phys.* **19**, 32184–32215 (2017).
22. Becke, A. D. Density-functional thermochemistry. III. The role of exact exchange. *J. Chem. Phys.* **98**, 5648–5652 (1993).
23. Stephens, P. J., Devlin, F. J., Chabalowski, C. F. & Frisch, M. J. Ab Initio Calculation of Vibrational Absorption and Circular Dichroism Spectra Using Density Functional Force Fields. *J. Phys. Chem.* **98**, 11623–11627 (1994).

24. Grimme, S., Ehrlich, S. & Goerigk, L. Effect of the damping function in dispersion corrected density functional theory. *J. Comput. Chem.* **32**, 1456–1465 (2011).
25. Adamo, C. & Barone, V. Toward reliable density functional methods without adjustable parameters: The PBE0 model. *J. Chem. Phys.* **110**, 6158–6170 (1999).
26. Ernzerhof, M. & Scuseria, G. E. Assessment of the Perdew–Burke–Ernzerhof exchange–correlation functional. *J. Chem. Phys.* **110**, 5029–5036 (1999).
27. Grimme, S., Ehrlich, S. & Goerigk, L. Effect of the damping function in dispersion corrected density functional theory. *J. Comput. Chem.* **32**, 1456–1465 (2011).
28. Chai, J.-D. & Head-Gordon, M. Long-range corrected hybrid density functionals with damped atom–atom dispersion corrections. *Phys. Chem. Chem. Phys.* **10**, 6615 (2008).
29. Zhao, Y. & Truhlar, D. G. The M06 suite of density functionals for main group thermochemistry, thermochemical kinetics, noncovalent interactions, excited states, and transition elements: two new functionals and systematic testing of four M06-class functionals and 12 other functionals. *Theor. Chem. Acc.* **120**, 215–241 (2008).
30. Goerigk, L. & Grimme, S. A thorough benchmark of density functional methods for general main group thermochemistry, kinetics, and noncovalent interactions. *Phys. Chem. Chem. Phys.* **13**, 6670 (2011).
31. Yu, H. S., He, X., Li, S. L. & Truhlar, D. G. MN15: A Kohn–Sham global-hybrid exchange–correlation density functional with broad accuracy for multi-reference and single-reference systems and noncovalent interactions. *Chem. Sci.* **7**, 5032–5051 (2016).
32. Grimme, S. Semiempirical hybrid density functional with perturbative second-order correlation. *J. Chem. Phys.* **124**, 034108 (2006).
33. Goerigk, L. & Grimme, S. A thorough benchmark of density functional methods for general main group thermochemistry, kinetics, and noncovalent interactions. *Phys. Chem. Chem. Phys.* **13**, 6670 (2011).
34. Kozuch, S. & Martin, J. M. L. DSD-PBEP86: in search of the best double-hybrid DFT with spin-component scaled MP2 and dispersion corrections. *Phys. Chem. Chem. Phys.* **13**, 20104 (2011).
35. Santra, G., Sylvetsky, N. & Martin, J. M. L. Minimally Empirical Double-Hybrid Functionals Trained against the GMTKN55 Database: revDSD-PBEP86-D4, revDOD-PBE-D4, and DOD-SCAN-D4. *J. Phys. Chem. A* **123**, 5129–5143 (2019).
36. Papajak, E. & Truhlar, D. G. Convergent Partially Augmented Basis Sets for Post-Hartree–Fock Calculations of Molecular Properties and Reaction Barrier Heights. *J. Chem. Theory Comput.* **7**, 10–18 (2011).
37. Woon, D. E. & Dunning, T. H. Gaussian basis sets for use in correlated molecular calculations. III. The atoms aluminum through argon. *J. Chem. Phys.* **98**, 1358–1371 (1993).
38. Dunning, T. H. Gaussian basis sets for use in correlated molecular calculations. I. The atoms boron through neon and hydrogen. *J. Chem. Phys.* **90**, 1007–1023 (1989).
39. Jeziorski, B., Moszynski, R. & Szalewicz, K. Perturbation Theory Approach to Intermolecular Potential Energy Surfaces of van der Waals Complexes. *Chem. Rev.* **94**, 1887–1930 (1994).
40. Smith, D. G. A. *et al.* PSI4 1.4:Open-source software for high-throughput quantum chemistry. *J. Chem. Phys.* **152**, 184108 (2020).
41. Parker, T. M., Burns, L. A., Parrish, R. M., Ryno, A. G. & Sherrill, C. D. Levels of symmetry

- adapted perturbation theory (SAPT). I. Efficiency and performance for interaction energies. *J. Chem. Phys.* **140**, 094106 (2014).
42. Szalewicz, K. Symmetry-adapted perturbation theory of intermolecular forces: Symmetry-adapted perturbation theory. *Wiley Interdiscip. Rev. Comput. Mol. Sci.* **2**, 254–272 (2012).
43. Kendall, R. A., Dunning, T. H. & Harrison, R. J. Electron affinities of the first-row atoms revisited. Systematic basis sets and wave functions. *J. Chem. Phys.* **96**, 6796–6806 (1992).
44. Woon, D. E. & Dunning, T. H. Gaussian basis sets for use in correlated molecular calculations. IV. Calculation of static electrical response properties. *J. Chem. Phys.* **100**, 2975–2988 (1994).
45. Woon, D. E. & Dunning, T. H. Gaussian basis sets for use in correlated molecular calculations. V. Core-valence basis sets for boron through neon. *J. Chem. Phys.* **103**, 4572–4585 (1995).
46. Lu, T. & Chen, Q. Shermo: A general code for calculating molecular thermochemistry properties. *Comput. Theor. Chem.* **1200**, 113249 (2021).
47. Neese, F. Software update: the ORCA program system, version 4.0. *WIREs Comput. Mol. Sci.* **8**, e1327 (2018).
48. Neese, F., Wennmohs, F., Becker, U. & Ripplinger, C. The ORCA quantum chemistry program package. *J. Chem. Phys.* **152**, 224108 (2020).
49. Weigend, F. & Ahlrichs, R. Balanced basis sets of split valence, triple zeta valence and quadruple zeta valence quality for H to Rn: Design and assessment of accuracy. *Phys. Chem. Chem. Phys.* **7**, 3297 (2005).
50. Kossmann, S. & Neese, F. Comparison of two efficient approximate Hartee–Fock approaches. *Chem. Phys. Lett.* **481**, 240–243 (2009).
51. Pickett, H. M. The fitting and prediction of vibration-rotation spectra with spin interactions. *J. Mol. Spectrosc.* **148**, 371–377 (1991).
52. Humphrey, W., Dalke, A. & Schulten, K. VMD: Visual molecular dynamics. *J. Mol. Graph.* **14**, 33–38 (1996).
53. Western, C. M. PGOPHER: A program for simulating rotational, vibrational and electronic spectra. *J. Quant. Spectrosc. Radiat. Transf.* **186**, 221–242 (2017).
54. Pu, L., Sun, Y. & Zhang, Z. Hydrogen Bonding in Hydrates with one Acetic Acid Molecule. *J. Phys. Chem. A* **114**, 10842–10849 (2010).
55. Stiefvater, O. L. Microwave spectrum of propionic acid. I. Spectrum, dipole moment, barrier to internal rotation, and low-frequency vibrations of cis-propionic acid. *J. Chem. Phys.* **62**, 233 (1975).
56. Townes, C. H. & Schawlow, A. L. *Microwave spectroscopy*. (Dover Publications, 1975).
57. Ouyang, B., Starkey, T. G. & Howard, B. J. High-Resolution Microwave Studies of Ring-Structured Complexes between Trifluoroacetic Acid and Water. *J. Phys. Chem. A* **111**, 6165–6175 (2007).
58. Puzzarini, C. & Barone, V. A never-ending story in the sky: The secrets of chemical evolution. *Phys. Life Rev.* **32**, 59–94 (2020).
59. Ramachandran, G. N. & Sasisekharan, V. Conformation of Polypeptides and Proteins**The literature survey for this review was completed in September 1967, with the journals which were then available in Madras and the preprinta which the authors had received.††By the authors' request, the publishers have left certain matters of usage and spelling in the form in which they

wrote them. in *Advances in Protein Chemistry* (eds. Anfinsen, C. B., Anson, M. L., Edsall, J. T. & Richards, F. M.) vol. 23 283–437 (Academic Press, 1968).

Supporting Information

1.Statistical measures of the data set

For a set of calculated data $\{a_1, a_2, \dots, a_n\}$ and the experimental reference data $\{b_1, b_2, \dots, b_n\}$ statistical measures are:

(1) Root mean square deviation (RMSD):

$$RMSD = \sqrt{\frac{1}{n} \sum_{i=1}^n |a_i - b_i|^2}$$

(2) Absolute deviation (ADEV):

$$AE = a_i - b_i$$

(3) Mean absolute deviation (MAD):

$$MAD = \frac{1}{n} \sum_{i=1}^n |a_i - b_i|$$

2.RMSD of optimized geometries

We used RMSD to measure geometric differences to check whether structures optimized with these methods are plausible. Taking the optimal rev-DSDPBEP86-D3(BJ) as the benchmark, the RMSDs of the coordinates of the optimized geometries calculated with different methods were summarized in **Table 3**. Despite being mediocre in calculating the rotational constants of SCFAs, MP2 and ω B97X-D are outstanding in calculating geometric structures. The rest of the ordinary functionals are not much different except for MN15L (D3), and HF has the worst performance.

Table S1 RMSDs of SCFAs geometries calculated with different methods relative to revDSD-PBEP86-D3(BJ)

RMSD(Å)	B2PLYP-D3(BJ)	B3LYP-D3(BJ)	BLYP-D3(BJ)	DSD-PBEP86-D3(BJ)	HF	M06-2X(D3)	MN15-D3(BJ)	MN15L(D3)	MP2	PBE0-D3(BJ)	ω B97XD
AA	0.016	0.005	0.005	0.008	0.004	0.005	0.002	0.004	0.016	0.001	0.005
AA-w	0.006	0.012	0.025	0.008	0.108	0.020	0.011	0.074	0.017	0.037	0.017
AA-w₂	0.008	0.126	0.025	0.030	0.102	0.029	0.043	0.009	0.020	0.036	0.023
PPA	0.002	0.018	0.008	0.012	0.013	0.006	0.005	0.004	0.009	0.022	0.007
PPA-w	0.103	0.019	0.017	0.068	0.012	0.034	0.006	0.011	0.026	0.008	0.017
PPA-w₂	0.009	0.021	0.041	0.008	0.116	0.029	0.031	0.095	0.012	0.041	0.022
BA	0.003	0.007	0.022	0.002	0.015	0.007	0.011	0.012	0.007	0.006	0.005
BA-w	0.005	0.010	0.026	0.008	0.094	0.018	0.013	0.065	0.012	0.033	0.015
BA-w₂	0.009	0.019	0.041	0.008	0.109	0.030	0.029	0.089	0.013	0.039	0.021
PTA	0.004	0.009	0.026	0.003	0.017	0.008	0.014	0.014	0.008	0.007	0.006
PTA-w	0.006	0.011	0.029	0.007	0.090	0.018	0.018	0.061	0.013	0.031	0.015
PTA-w₂	0.010	0.021	0.046	0.008	0.103	0.035	0.035	0.089	0.015	0.037	0.022
HXA	0.004	0.008	0.028	0.003	0.015	0.008	0.013	0.014	0.008	0.008	0.005
HXA-w	0.005	0.010	0.031	0.007	0.084	0.017	0.016	0.059	0.013	0.030	0.014

HXA-w₂	0.009	0.020	0.047	0.008	0.097	0.035	0.034	0.085	0.015	0.036	0.021
Average	0.013	0.021	0.028	0.013	0.065	0.020	0.019	0.046	0.013	0.025	0.014

3. Rotational constants, centrifugal distortion constants and dipole moment of SCFAs and corresponding water clusters (except for PTA-w) calculated with twelve different methods

Table S2.1 Rotational constants, centrifugal distortion constants and dipole moment of AA calculated with twelve different methods

Parameters	Experiment	B2PLYP-D3(BJ)	B3LYP-D3(BJ)	BLYP-D3(BJ)	DSD-PBEP86-D3(BJ)	HF	M06-2X(D3)	MN15-D3(BJ)	MN15L(D3)	MP2	PBE0-D3(BJ)	revDSD-PBEP86-D3(BJ)	ω B97X-D
A (MHz)	11335.47	11331.3380	11354.3677	11074.9837	11339.7891	11772.1531	11466.0607	11458.9316	11292.6789	11293.0493	11451.7509	11327.7036	11466.6232
B (MHz)	9478.604	9499.3886	9481.9171	9329.9409	9507.2454	9602.8684	9531.7030	9512.7027	9425.5035	9530.1354	9558.2884	9492.0740	9523.8773
C (MHz)	5324.906	5336.6727	5336.5581	5228.5165	5341.9304	5464.8743	5377.1375	5369.2065	5307.7079	5337.8268	5382.4041	5334.6625	5374.7139
A_J (kHz)	N/A	9446.064	9481.687	9776.197	9337.806	8655.907	9212.378	9571.894	9013.473	9340.936	9375.644	9339.099	9312.217
A_K (kHz)	N/A	-8035.385	-3533.547	-3978.007	-4108.203	-662.922	-2731.057	-1632.531	-3371.541	-20423.482	-3541.590	-4417.788	-3684.501
A_h (kHz)	N/A	-569.356	-5100.388	-4916.918	-4400.892	-7206.578	-5664.919	-7122.248	-4846.207	11907.662	-5008.746	-4090.709	-4796.019
δ_J (kHz)	N/A	676.434	665.809	687.381	667.086	602.456	636.306	710.378	624.922	666.783	661.747	664.119	661.007
δ_K (kHz)	N/A	4035.855	5612.186	5316.169	6496.997	5959.211	6650.158	8207.777	8702.987	-1045.800	6562.557	6288.031	5777.826
μ_e (D)	0.76	0.79	0.88	0.89	0.77	0.91	0.89	0.87	0.89	0.75	0.87	0.76	0.87
μ_b (D)	1.46	1.54	1.55	1.48	1.53	1.74	1.55	1.58	1.57	1.45	1.58	1.52	1.59
μ_c (D)	0.00	0.00	0.00	0.00	0.00	0.00	0.00	0.00	0.00	0.00	0.00	0.00	0.00
μ_{tor} (D)	1.7	1.73	1.78	1.72	1.71	1.96	1.79	1.80	1.81	1.63	1.80	1.70	1.81

Table S2.2 Rotational constants, centrifugal distortion constants and dipole moment of AA-w calculated with twelve different methods

Parameters	Experiment	B2PLYP-D3(BJ)	B3LYP-D3(BJ)	BLYP-D3(BJ)	DSD-PBEP86-D3(BJ)	HF	M06-2X(D3)	MN15-D3(BJ)	MN15L(D3)	MP2	PBE0-D3(BJ)	revDSD-PBEP86-D3(BJ)	ω B97X-D
A (MHz)	11059.8286	11036.3939	11060.6092	10792.0194	11041.1119	11481.2759	11162.3810	11148.3107	10971.7582	11006.3978	11149.7825	11029.8567	11155.2643
B (MHz)	2584.53109	2645.7208	2646.3109	2617.5750	2650.5678	2453.8643	2635.6970	2632.4780	2474.2669	2655.5473	2700.2312	2631.6705	2631.4093
C (MHz)	2127.47530	2171.1810	2172.9801	2144.6421	2174.9874	2051.9078	2168.0917	2165.9459	2052.1173	2176.0837	2213.4167	2161.8049	2166.8892
A_J (kHz)	1.29	1183.167	1157.570	1161.696	1190.441	1587.217	1212.459	1235.178	1407.634	1243.645	1170.474	1217.337	1201.698
A_K (kHz)	N/A	5372.826	5291.078	5553.558	5352.061	1988.127	5122.312	5755.144	4897.632	5471.302	5408.876	5228.264	4807.190
A_{JK} (kHz)	3.38	2392.629	2403.949	2269.261	2318.571	5377.145	2570.245	2076.996	2820.726	2299.680	2085.443	2444.342	2763.427
δ_J (kHz)	0.271	226.055	220.593	223.119	227.492	275.935	230.079	234.522	256.507	238.149	224.598	231.364	226.793
δ_K (kHz)	N/A	1298.764	1626.398	727.025	1350.052	5386.752	2809.820	2631.054	3292.875	597.491	1303.812	1677.164	2115.216
μ_e (D)	0.2-0.3	0.44	0.52	0.61	0.42	0.19	0.32	0.39	0.26	0.33	0.55	0.41	0.52
μ_b (D)	0.2	0.25	0.31	0.31	0.24	0.27	0.23	0.27	0.32	0.15	0.35	0.23	0.34
μ_c (D)	N/A	1.22	1.24	1.27	1.23	1.02	1.16	1.20	1.15	1.18	1.27	1.22	1.26
μ_{tor} (D)	N/A	1.32	1.38	1.44	1.32	1.07	1.23	1.29	1.22	1.23	1.43	1.31	1.41

Table S2.3 Rotational constants, centrifugal distortion constants and dipole moment of AA-w₂ calculated with twelve different methods

Parameters	Experiment	B2PLYP-D3(BJ)	B3LYP-D3(BJ)	BLYP-D3(BJ)	DSD-PBEP86-D3(BJ)	HF	M06-2X(D3)	MN15-D3(BJ)	MN15L(D3)	MP2	PBE0-D3(BJ)	revDSD-PBEP86-D3(BJ)	ω B97X-D
A (MHz)	4445.466	4498.0012	4510.7249	4447.5348	4500.8261	4279.3482	4532.9982	4481.1428	4236.2670	4494.3074	4584.6877	4477.9266	4518.6978
B (MHz)	1618.43953	1645.7909	1654.0597	1636.4068	1646.1454	1546.1384	1651.1492	1627.3078	1531.0366	1645.1127	1681.1677	1636.7481	1649.4601
C (MHz)	1199.67784	1218.8660	1224.6847	1211.2463	1219.4890	1145.8735	1224.3032	1207.0002	1137.4458	1218.2618	1245.4942	1212.6185	1223.2403

A_J (kHz)	0.364	289.324	279.269	278.232	294.530	392.075	318.178	311.055	376.118	309.538	286.625	299.265	286.268
A_K (kHz)	N/A	542.263	530.721	503.826	533.401	1861.030	530.545	306.057	752.670	603.630	502.546	614.845	624.375
A_{JK} (kHz)	4.20	3268.063	3136.715	2975.276	3349.313	4354.608	3881.799	3983.836	5047.041	3451.922	3137.106	3368.858	3176.649
δ_J (kHz)	0.0788	64.319	61.529	60.720	65.111	90.846	68.353	69.366	81.649	67.870	62.411	66.328	62.716
δ_K (kHz)	2.76	1668.891	1634.757	1473.736	1722.752	2514.558	2098.945	2200.897	2842.248	1714.998	1626.777	1767.259	1724.531
$ \mu_e $ (D)	0.2-0.3	0.25	0.32	0.36	0.24	0.27	0.20	0.19	0.32	0.16	0.30	0.24	0.38
$ \mu_b $ (D)	<0.1	0.03	0.07	0.07	0.01	0.04	0.03	0.04	0.00	0.06	0.10	0.00	0.07
$ \mu_c $ (D)	N/A	2.18	2.23	2.31	2.20	1.66	2.13	2.08	2.10	2.14	2.29	2.19	2.26
$ \mu_{tot} $ (D)	N/A	2.20	2.25	2.34	2.22	1.68	2.14	2.09	2.12	2.15	2.31	2.21	2.29

Table S2.4 Rotational constants, centrifugal distortion constants and dipole moment of PPA calculated with twelve different methods

Parameter s	Experiment	B2PLYP-D3(BJ)	B3LYP-D3(BJ)	BLYP-D3(BJ)	DSD-PBEP86-D3(BJ)	HF	M06-2X(D3)	MN15-D3(BJ)	MN15L(D3)	MP2	PBE0-D3(BJ)	revDSD-PBEP86-D3(BJ)	ω B97X-D
A (MHz)	10,155.38	10180.1036	10201.2675	9980.3165	10177.8194	10510.9915	10289.1544	10277.2007	10091.5021	10145.1818	10269.7348	10166.6671	10278.2855
B (MHz)	3,817.89	3823.6489	3809.1360	3742.3173	3837.1509	3842.0012	3851.3407	3859.4848	3818.5616	3850.4956	3849.9794	3828.7849	3829.6043
C (MHz)	2,875.17	2876.8315	2870.4162	2816.1146	2884.7982	2912.3757	2901.4243	2904.9340	2868.7878	2889.2621	2899.1084	2879.3153	2888.1554
A_J (kHz)	0.685	754.751	751.864	761.116	756.633	692.510	749.130	779.128	729.262	761.787	768.495	755.471	746.535
A_K (kHz)	2.89	3026.239	3107.928	3087.101	3030.146	2979.709	3301.862	3501.249	3188.791	2938.086	3012.953	3037.365	3092.001
A_{JK} (kHz)	3.78	3548.039	3479.770	3680.852	3475.076	3031.833	3142.119	3275.279	3112.626	3564.123	3516.084	3463.778	3393.546
δ_J (kHz)	-0.1866	188.105	186.851	189.174	189.149	169.804	187.462	195.773	183.326	191.217	191.728	188.713	185.661
δ_K (kHz)	-0.0076	-226.002	65.034	-472.524	11.586	554.702	829.313	956.775	977.410	-359.582	162.774	55.322	42.653
$ \mu_e $ (D)	0.19	0.18	0.15	0.23	0.14	0.16	0.16	0.09	0.04	0.16	0.13	0.15	0.13
$ \mu_b $ (D)	1.53	1.59	1.56	1.58	1.56	1.82	1.64	1.65	1.66	1.49	1.65	1.56	1.67
$ \mu_c $ (D)	0.00	0.00	0.00	0.00	0.00	0.00	0.00	0.00	0.00	0.00	0.00	0.00	0.00
$ \mu_{tot} $ (D)	1.54	1.60	1.57	1.60	1.57	1.82	1.64	1.65	1.66	1.50	1.66	1.56	1.68

Table S2.5 Rotational constants, centrifugal distortion constants and dipole moment of PPA-w calculated with twelve different methods

Parameter s	Experiment	B2PLYP-D3(BJ)	B3LYP-D3(BJ)	BLYP-D3(BJ)	DSD-PBEP86-D3(BJ)	HF	M06-2X(D3)	MN15-D3(BJ)	MN15L(D3)	MP2	PBE0-D3(BJ)	revDSD-PBEP86-D3(BJ)	ω B97X-D
A (MHz)	8,167.31	8193.7784	8212.6059	8042.3866	8189.0616	8412.1626	8232.1756	8205.1112	8039.9723	8171.4096	8288.2501	8179.0910	8270.5710
B (MHz)	1,618.81	1646.7225	1644.0013	1622.5808	1651.9176	1554.2992	1649.2113	1651.3609	1571.5648	1656.5415	1673.3163	1641.8665	1639.1736
C (MHz)	1,377.16	1398.0436	1396.8327	1377.1568	1401.8540	1335.1135	1400.4938	1401.4404	1339.5501	1404.4276	1420.4550	1394.3366	1395.1658
A_J (kHz)	0.4115	349.824	341.485	338.988	353.318	463.522	350.753	368.019	406.661	367.444	347.290	360.593	350.884
A_K (kHz)	N/A	13066.437	13048.694	12439.221	12877.369	23656.485	13440.350	13090.659	15685.596	12900.575	12302.475	13331.862	13304.101
A_{JK} (kHz)	-0.903	-621.822	-608.119	-514.784	-642.364	-883.905	-439.863	-623.294	-364.161	-660.643	-682.205	-662.582	-764.830
δ_J (kHz)	-0.0757	64.166	62.496	61.725	64.939	81.014	63.497	67.327	71.051	67.501	63.914	66.068	64.382
δ_K (kHz)	-0.0071	606.272	644.681	557.048	624.443	1330.522	799.604	841.196	1101.774	529.817	625.292	664.579	666.157
$ \mu_e $ (D)	N/A	0.45	0.54	0.63	0.43	0.23	0.34	0.37	0.22	0.36	0.54	0.41	0.52
$ \mu_b $ (D)	N/A	0.19	0.26	0.28	0.18	0.16	0.14	0.19	0.23	0.09	0.31	0.16	0.30
$ \mu_c $ (D)	N/A	1.22	1.24	1.27	1.23	1.02	1.16	1.19	1.15	1.21	1.27	1.23	1.26
$ \mu_{tot} $ (D)	N/A	1.32	1.38	1.45	1.31	1.06	1.22	1.26	1.20	1.26	1.42	1.30	1.40

Table S2.6 Rotational constants, centrifugal distortion constants and dipole moment of PPA-w2 calculated with twelve different methods

Parameter	Experiment	B2PLYP-D3(BJ)	B3LYP-D3(BJ)	BLYP-D3(BJ)	DSD-PBEP86-D3(BJ)	HF	M06-2X(D3)	MN15-D3(BJ)	MN15L(D3)	MP2	PBE0-D3(BJ)	revDSD-PBEP86-D3(BJ)	ω B97X-D
A (MHz)	3,627.72	3706.0613	3736.4046	3703.4859	3694.2053	3491.0056	3666.4130	3626.5857	3360.4212	3681.0892	3783.5229	3674.6566	3727.9567
B (MHz)	1,102.65	1112.1951	1112.2212	1095.6428	1115.5885	1064.8392	1127.8289	1116.5197	1074.6587	1117.6333	1130.3121	1109.7073	1112.8593
C (MHz)	857.26038	867.0414	868.8696	857.5043	868.5882	825.2324	874.2157	865.1006	825.1862	868.9049	882.6898	863.9255	869.0290
A_J (kHz)	0.145	130.321	124.720	120.770	133.880	181.119	149.680	153.970	193.026	138.636	126.851	135.963	129.391
A_K (kHz)	N/A	3534.372	3416.831	3213.924	3591.334	5280.822	4224.068	4246.654	5682.303	3641.721	3374.421	3652.316	3604.883
A_{JK} (kHz)	0.692	541.365	515.994	528.617	554.717	662.033	601.667	545.434	599.917	599.739	536.877	560.144	514.953
δ_J (kHz)	-0.0415	31.448	29.750	27.900	32.410	46.435	37.203	39.623	52.965	33.436	29.876	32.948	31.062
δ_K (kHz)	-0.00841	554.938	529.363	493.861	575.351	817.054	687.033	703.488	916.871	585.756	536.232	583.587	561.062
$ \mu_a $ (D)	N/A	0.29	0.36	0.42	0.28	0.32	0.25	0.21	0.33	0.22	0.34	0.29	0.42
$ \mu_b $ (D)	N/A	0.07	0.02	0.00	0.08	0.04	0.13	0.08	0.04	0.16	0.02	0.09	0.01
$ \mu_c $ (D)	N/A	2.18	2.23	2.32	2.20	1.66	2.14	2.09	2.12	2.16	2.29	2.19	2.27
$ \mu_{tot} $ (D)	N/A	2.20	2.26	2.35	2.22	1.69	2.16	2.10	2.14	2.18	2.32	2.21	2.31

Table S2.7 Rotational constants, centrifugal distortion constants and dipole moment of BA calculated with twelve different methods

Parameters	B2PLYP-D3(BJ)	B3LYP-D3(BJ)	BLYP-D3(BJ)	DSD-PBEP86-D3(BJ)	HF	M06-2X(D3)	MN15-D3(BJ)	MN15L(D3)	MP2	PBE0-D3(BJ)	revDSD-PBEP86-D3(BJ)	ω B97X-D
A (MHz)	9022.7857	9040.2067	8843.9453	9021.4938	9304.9207	9116.0935	9110.4725	8943.4974	8991.8901	9106.7159	9011.3326	9107.1481
B (MHz)	1837.3317	1830.9973	1801.1479	1842.7817	1842.2081	1848.0618	1853.0546	1831.3333	1849.1586	1848.7194	1838.9146	1839.4005
C (MHz)	1570.2262	1566.1589	1538.9444	1574.3951	1581.7415	1580.9749	1584.4086	1564.3605	1577.9612	1581.1601	1571.3229	1574.3373
A_J (kHz)	142.856	142.646	144.891	142.982	130.316	141.823	147.962	137.969	144.059	144.698	142.760	141.092
A_K (kHz)	4381.479	4404.951	4482.283	4334.067	4056.244	4406.452	4681.089	4245.727	4325.496	4369.992	4330.698	4307.297
A_{JK} (kHz)	1452.466	1434.370	1492.573	1457.810	1254.524	1381.337	1440.858	1328.603	1488.604	1482.796	1451.737	1421.521
δ_J (kHz)	21.822	21.708	22.149	21.887	19.357	21.637	22.778	21.301	22.209	22.041	21.830	21.422
δ_K (kHz)	-848.764	-832.792	-1566.435	-889.960	-235.645	-294.363	-187.054	-22.582	-1198.246	-748.573	-851.054	-1194.729
$ \mu_a $ (D)	0.51	0.52	0.57	0.47	0.52	0.50	0.43	0.38	0.47	0.47	0.47	0.48
$ \mu_b $ (D)	1.44	1.49	1.42	1.42	1.67	1.49	1.51	1.51	1.35	1.51	1.42	1.53
$ \mu_c $ (D)	0.00	0.00	0.00	0.00	0.00	0.00	0.00	0.00	0.00	0.00	0.00	0.00
$ \mu_{tot} $ (D)	1.53	1.58	1.53	1.50	1.75	1.58	1.57	1.56	1.43	1.58	1.49	1.60

Table S2.8 Rotational constants, centrifugal distortion constants and dipole moment of BA-w calculated with twelve different methods

BA-w	B2PLYP-D3(BJ)	B3LYP-D3(BJ)	BLYP-D3(BJ)	DSD-PBEP86-D3(BJ)	HF	M06-2X(D3)	MN15-D3(BJ)	MN15L(D3)	MP2	PBE0-D3(BJ)	revDSD-PBEP86-D3(BJ)	ω B97X-D
A (MHz)	7829.5115	7844.2604	7689.5433	7826.0896	8016.4654	7864.9509	7846.3049	7681.3671	7815.3657	7913.3629	7815.0047	7897.2300
B (MHz)	967.9590	965.9692	952.5757	970.7453	929.4303	970.3324	971.8073	934.5152	973.3060	980.8581	966.0161	965.3186
C (MHz)	876.6702	875.2956	862.7138	879.0192	846.4811	878.8888	879.9548	847.5953	880.8855	888.4935	875.0137	875.4774
A_J (kHz)	78.189	76.439	76.250	78.881	101.802	78.687	82.338	90.470	81.704	77.463	80.363	78.836
A_K (kHz)	12346.944	12234.202	11592.211	12190.859	23293.460	13099.204	12657.127	15938.258	12264.943	11406.205	12648.301	12362.345
A_{JK} (kHz)	-318.529	-307.676	-262.466	-328.487	-622.115	-291.257	-335.767	-314.530	-332.651	-315.684	-343.932	-380.783
δ_J (kHz)	9.482	9.245	9.152	9.587	12.106	9.469	10.014	10.538	9.901	9.407	9.750	9.622
δ_K (kHz)	-175.727	-95.006	-236.122	-139.249	165.482	56.831	98.839	167.472	-336.765	-81.009	-116.326	-79.884
$ \mu_a $ (D)	0.51	0.59	0.69	0.48	0.28	0.39	0.42	0.25	0.42	0.60	0.47	0.57
$ \mu_b $ (D)	0.09	0.17	0.18	0.08	0.06	0.05	0.10	0.11	0.00	0.22	0.07	0.21

$ \mu_e $ (D)	1.22	1.24	1.27	1.23	1.02	1.16	1.20	1.15	1.21	1.27	1.22	1.26
$ \mu_{rot} $ (D)	1.32	1.38	1.46	1.32	1.06	1.22	1.27	1.18	1.28	1.42	1.31	1.40

Table S2.9 Rotational constants, centrifugal distortion constants and dipole moment of BA-w₂ calculated with twelve different methods

Parameters	B2PLYP-D3(BJ)	B3LYP-D3(BJ)	BLYP-D3(BJ)	DSD-PBEP86-D3(BJ)	HF	M06-2X(D3)	MN15-D3(BJ)	MN15L(D3)	MP2	PBE0-D3(BJ)	revDSD-PBEP86-D3(BJ)	ω B97X-D
<i>A</i> (MHz)	3592.9077	3624.1269	3598.6807	3579.1810	3370.1953	3541.4690	3502.6142	3228.7497	3565.7799	3667.8939	3559.6124	3614.4992
<i>B</i> (MHz)	694.4808	693.7836	683.0176	696.6179	672.9480	703.4655	698.6989	677.7988	698.0926	704.1223	693.5357	694.9802
<i>C</i> (MHz)	589.4336	589.8396	581.6484	590.6745	567.2414	594.4675	589.9072	567.3876	591.2764	598.5800	587.9198	590.5375
<i>A_J</i> (kHz)	39.464	37.688	36.325	40.584	55.022	45.740	47.280	62.239	41.992	38.298	41.187	39.087
<i>A_K</i> (kHz)	4799.566	4573.004	4240.510	4925.045	7136.393	5885.152	6001.041	8330.501	5051.887	4562.659	5001.265	4809.002
<i>A_{JK}</i> (kHz)	57.223	63.914	99.534	50.772	-24.837	-12.715	-47.058	-206.092	64.523	74.256	51.082	56.480
δ_J (kHz)	7.556	7.078	6.516	7.832	11.578	9.234	9.982	14.750	8.092	7.103	7.964	7.399
δ_K (kHz)	147.583	151.037	115.962	160.296	262.207	213.952	221.831	298.770	138.321	157.758	165.787	174.549
$ \mu_e $ (D)	0.34	0.40	0.46	0.32	0.36	0.30	0.24	0.35	0.26	0.37	0.33	0.46
$ \mu_b $ (D)	0.15	0.09	0.08	0.17	0.12	0.23	0.17	0.15	0.25	0.06	0.17	0.06
$ \mu_c $ (D)	2.18	2.23	2.32	2.20	1.67	2.14	2.09	2.12	2.16	2.29	2.19	2.27
$ \mu_{rot} $ (D)	2.21	2.27	2.36	2.23	1.71	2.17	2.12	2.16	2.19	2.32	2.23	2.31

Table S2.10 Rotational constants, centrifugal distortion constants and dipole moment of PTA calculated with twelve different methods

Parameters	B2PLYP-D3(BJ)	B3LYP-D3(BJ)	BLYP-D3(BJ)	DSD-PBEP86-D3(BJ)	HF	M06-2X(D3)	MN15-D3(BJ)	MN15L(D3)	MP2	PBE0-D3(BJ)	revDSD-PBEP86-D3(BJ)	ω B97X-D
<i>A</i> (MHz)	7991.8900	8007.6913	7850.3819	7983.3497	8218.6240	8053.6516	8042.3390	7898.6245	7962.7461	8055.8492	7974.9854	8057.3717
<i>B</i> (MHz)	1052.1225	1048.1039	1030.7338	1055.3432	1052.4925	1058.6487	1062.0915	1048.3243	1059.0208	1058.8714	1053.1017	1053.1948
<i>C</i> (MHz)	951.2569	948.2069	932.0382	953.8800	954.4836	957.5086	960.1512	947.2912	956.5074	957.7153	951.9581	953.0833
<i>A_J</i> (kHz)	47.391	47.060	47.500	47.668	42.613	47.308	50.089	46.181	48.218	48.305	47.532	46.588
<i>A_K</i> (kHz)	3355.895	3361.243	3400.967	3347.380	3134.674	3368.872	3607.009	3338.498	3342.794	3381.046	3342.571	3333.752
<i>A_{JK}</i> (kHz)	505.321	495.893	518.034	498.136	423.434	461.301	484.374	450.997	509.937	507.290	497.260	475.481
δ_J (kHz)	5.102	5.031	5.071	5.163	4.461	5.120	5.498	5.063	5.261	5.216	5.141	4.988
δ_K (kHz)	-433.436	-290.248	-622.151	-330.921	-105.416	-30.951	-48.363	-35.492	-450.542	-278.512	-339.199	-169.411
$ \mu_e $ (D)	0.39	0.41	0.47	0.35	0.39	0.39	0.31	0.26	0.36	0.35	0.35	0.36
$ \mu_b $ (D)	1.54	1.59	1.53	1.52	1.77	1.59	1.60	1.62	1.44	1.61	1.51	1.62
$ \mu_c $ (D)	0.00	0.00	0.00	0.00	0.00	0.00	0.00	0.00	0.00	0.00	0.00	0.00
$ \mu_{rot} $ (D)	1.59	1.64	1.60	1.56	1.81	1.63	1.63	1.64	1.49	1.65	1.55	1.66

Table S2.11 Rotational constants, centrifugal distortion constants and dipole moment of PTA-w₂ calculated with twelve different methods

Parameters	B2PLYP-D3(BJ)	B3LYP-D3(BJ)	BLYP-D3(BJ)	DSD-PBEP86-D3(BJ)	HF	M06-2X(D3)	MN15-D3(BJ)	MN15L(D3)	MP2	PBE0-D3(BJ)	revDSD-PBEP86-D3(BJ)	ω B97X-D
<i>A</i> (MHz)	3091.2893	3123.6539	3111.1456	3073.1496	2892.1505	3020.5256	2987.2235	2736.2012	3057.7976	3158.3475	3056.5061	3111.8644
<i>B</i> (MHz)	479.0538	477.9187	469.9829	480.9284	468.0973	486.1966	484.1985	473.1926	482.3601	484.6365	479.0341	479.2826
<i>C</i> (MHz)	419.6253	419.3825	413.1947	420.7689	407.1309	423.7430	421.5228	408.1616	421.5325	425.2377	419.0049	420.2871
<i>A_J</i> (kHz)	20.586	19.583	18.752	21.256	27.157	24.076	25.097	32.439	22.082	20.058	21.448	20.369

A_x (kHz)	5945.184	5729.936	5443.093	6048.377	7839.400	7094.152	6965.063	8732.798	6201.762	5761.545	6096.127	5977.159
A_{Jx} (kHz)	-224.362	-209.585	-178.256	-235.251	-317.721	-308.197	-328.230	-473.490	-236.319	-210.583	-235.032	-219.037
δ_J (kHz)	4.248	3.964	3.670	4.430	6.010	5.344	5.635	8.134	4.629	4.038	4.470	4.165
δ_x (kHz)	69.185	74.013	59.697	76.460	123.333	101.569	108.698	143.998	54.572	76.901	79.791	54.007
$ \mu_a $ (D)	0.41	0.47	0.53	0.39	0.42	0.37	0.31	0.41	0.34	0.43	0.40	0.52
$ \mu_b $ (D)	0.07	0.00	0.02	0.09	0.02	0.15	0.08	0.03	0.17	0.03	0.09	0.02
$ \mu_c $ (D)	2.17	2.23	2.30	2.19	1.66	2.12	2.09	2.10	2.15	2.29	2.19	2.25
$ \mu_{tot} $ (D)	2.21	2.27	2.37	2.23	1.72	2.15	2.11	2.14	2.18	2.33	2.22	2.31

Table S2.12 Rotational constants, centrifugal distortion constants and dipole moment of HXA calculated with twelve different methods

Parameters	B2PLYP-D3(BJ)	B3LYP-D3(BJ)	BLYP-D3(BJ)	DSD-PBEP86-D3(BJ)	HF	M06-2X(D3)	MN15-D3(BJ)	MN15L(D3)	MP2	PBE0-D3(BJ)	revDSD-PBEP86-D3(BJ)	ω B97X-D
A (MHz)	7420.5676	7432.6209	7287.1353	7413.8716	7617.6190	7480.1767	7471.6472	7335.6920	7398.4917	7478.1352	7404.9191	7476.3561
B (MHz)	651.5545	649.1713	638.6964	653.4767	651.5206	655.0984	657.3631	648.3649	655.4775	655.7523	651.9489	652.4109
C (MHz)	610.0886	608.0852	598.0515	611.7872	611.2455	613.6205	615.5446	606.9627	613.3958	614.1785	610.4004	611.2282
A_J (kHz)	14.238	14.209	14.405	14.260	12.885	14.199	14.856	13.687	14.368	14.445	14.228	14.044
A_x (kHz)	2602.914	2610.049	2696.710	2571.260	2343.550	2540.300	2691.906	2485.311	2596.983	2577.176	2568.083	2553.751
A_{Jx} (kHz)	306.312	299.093	304.499	307.581	258.956	293.836	317.763	295.723	312.688	313.657	304.687	292.265
δ_J (kHz)	0.912	0.907	0.924	0.915	0.803	0.908	0.957	0.880	0.928	0.923	0.913	0.896
δ_x (kHz)	-272.959	-214.600	-370.263	-234.898	-110.476	-68.797	-92.539	-58.628	-235.016	-201.212	-213.837	-201.842
$ \mu_a $ (D)	0.49	0.51	0.57	0.45	0.49	0.48	0.40	0.36	0.46	0.45	0.45	0.46
$ \mu_b $ (D)	1.43	1.48	1.41	1.41	1.66	1.48	1.49	1.48	1.34	1.50	1.40	1.51
$ \mu_c $ (D)	0.00	0.00	0.00	0.00	0.00	0.00	0.00	0.00	0.00	0.00	0.00	0.00
$ \mu_{tot} $ (D)	1.51	1.56	1.52	1.48	1.73	1.56	1.54	1.53	1.41	1.56	1.48	1.58

Table S2.13 Rotational constants, centrifugal distortion constants and dipole moment of HXA-w calculated with twelve different methods

Parameters	B2PLYP-D3(BJ)	B3LYP-D3(BJ)	BLYP-D3(BJ)	DSD-PBEP86-D3(BJ)	HF	M06-2X(D3)	MN15-D3(BJ)	MN15L(D3)	MP2	PBE0-D3(BJ)	revDSD-PBEP86-D3(BJ)	ω B97X-D
A (MHz)	6063.3387	6076.3604	5975.2623	6053.1419	6139.2430	6058.9487	6040.2879	5891.3972	6051.7422	6127.8848	6043.3565	6109.1446
B (MHz)	426.0936	424.9325	418.6466	427.3358	415.8155	427.9117	429.0396	416.7897	428.6385	430.5302	425.7664	425.5990
C (MHz)	403.3137	402.3455	396.3619	404.4163	394.2585	404.8887	405.8328	394.3126	405.5511	407.6157	402.9707	403.0990
A_J (kHz)	10.040	9.870	9.856	10.139	11.645	10.170	10.687	10.942	10.374	10.075	10.235	9.973
A_x (kHz)	17345.106	17168.547	16435.096	17269.169	27817.756	18508.331	18541.633	21567.944	17365.829	16682.440	17685.174	17100.083
A_{Jx} (kHz)	-276.057	-270.960	-252.506	-279.968	-394.304	-283.523	-301.982	-302.382	-282.070	-277.078	-285.471	-284.343
δ_J (kHz)	0.965	0.945	0.928	0.978	1.132	0.994	1.057	1.053	0.997	0.972	0.988	0.961
δ_x (kHz)	-72.002	-51.818	-112.793	-53.805	14.000	-64.294	0.529	19.888	-110.569	-48.101	-50.547	-108.253
$ \mu_a $ (D)	0.56	0.64	0.74	0.53	0.33	0.44	0.46	0.28	0.47	0.64	0.51	0.61
$ \mu_b $ (D)	0.11	0.19	0.22	0.10	0.06	0.05	0.11	0.10	0.01	0.24	0.09	0.23
$ \mu_c $ (D)	1.21	1.24	1.26	1.23	1.02	1.16	1.19	1.15	1.20	1.27	1.22	1.26
$ \mu_{tot} $ (D)	1.34	1.40	1.48	1.34	1.08	1.24	1.28	1.18	1.29	1.44	1.33	1.41

Table S2.14 Rotational constants, centrifugal distortion constants and dipole moment of HXA-w2 calculated with twelve different methods

Parameters	B2PLYP-D3(BJ)	B3LYP-D3(BJ)	BLYP-D3(BJ)	DSD-PBEP86-D3(BJ)	HF	M06-2X(D3)	MN15-D3(BJ)	MN15L(D3)	MP2	PBE0-D3(BJ)	revDSD-PBEP86-D3(BJ)	ω B97X-D
------------	---------------	--------------	-------------	-------------------	----	------------	-------------	-----------	-----	-------------	----------------------	-----------------

	3029.1023	3062.5116	3050.5958	3011.4970	2831.8023	2956.9422	2925.3332	2675.2749	2997.3882	3094.5562	2995.0238	3048.3936
A (MHz)	330.3368	329.4451	324.0266	331.5228	324.2886	334.6521	333.7884	326.8797	332.5010	333.8362	330.3410	330.5864
B (MHz)	300.8998	300.5021	295.9637	301.7329	293.6923	303.7347	302.6673	294.2963	302.3796	304.4946	300.5876	301.3531
A_J (kHz)	7.716	7.358	7.057	7.948	10.040	8.981	9.402	11.897	8.236	7.526	8.020	7.545
A_K (kHz)	6197.385	5966.631	5645.396	6314.753	8128.109	7459.825	7350.997	9069.936	6492.964	6012.564	6365.046	6146.245
A_{JK} (kHz)	-132.021	-122.298	-101.945	-138.595	-196.582	-188.376	-198.099	-285.153	-139.576	-122.409	-139.026	-124.300
δ_1 (kHz)	1.277	1.189	1.095	1.331	1.823	1.635	1.722	2.486	1.388	1.211	1.345	1.234
δ_k (kHz)	36.807	39.500	27.278	41.621	69.488	54.899	65.403	83.988	20.391	45.374	43.284	7.836
$ \mu_a $ (D)	0.41	0.47	0.53	0.40	0.43	0.37	0.31	0.41	0.34	0.44	0.40	0.52
$ \mu_b $ (D)	0.15	0.08	0.07	0.17	0.11	0.23	0.17	0.13	0.25	0.05	0.17	0.05
$ \mu_c $ (D)	2.18	2.23	2.31	2.20	1.67	2.12	2.09	2.12	2.15	2.29	2.19	2.26
$ \mu_{rot} $ (D)	2.22	2.28	2.37	2.24	1.73	2.16	2.12	2.16	2.19	2.33	2.23	2.32

4. Benchmark data of evaluating the optimal method for calculating rotational constants

Figure S1 The absolute errors for rotational constant B of AA, AA-w, AA-w₂, PPA, PPA-w, and PPA-w₂ by using twelve methods (may-cc-pVTZ basis set)

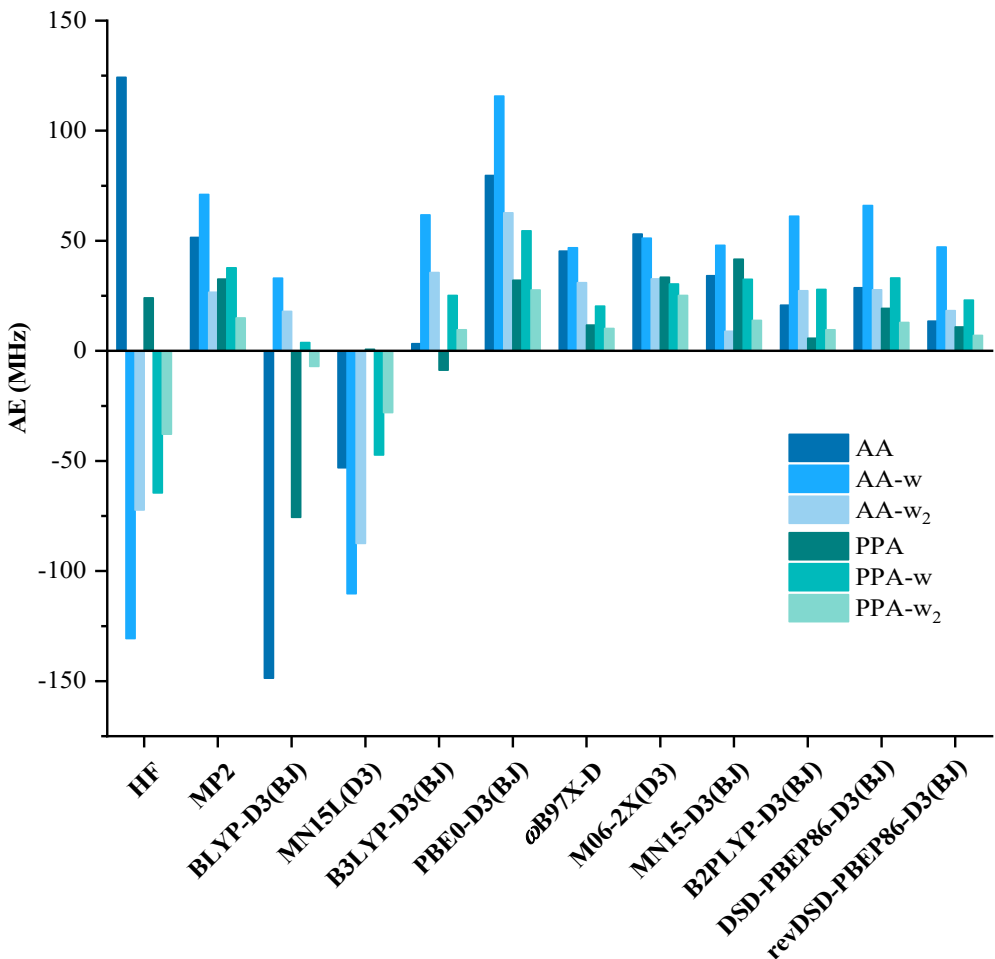


Figure S2 The absolute errors for rotational constant C of AA, AA-w, AA-w₂, PPA, PPA-w, and PPA-w₂ by using twelve methods (may-cc-pVTZ basis set)

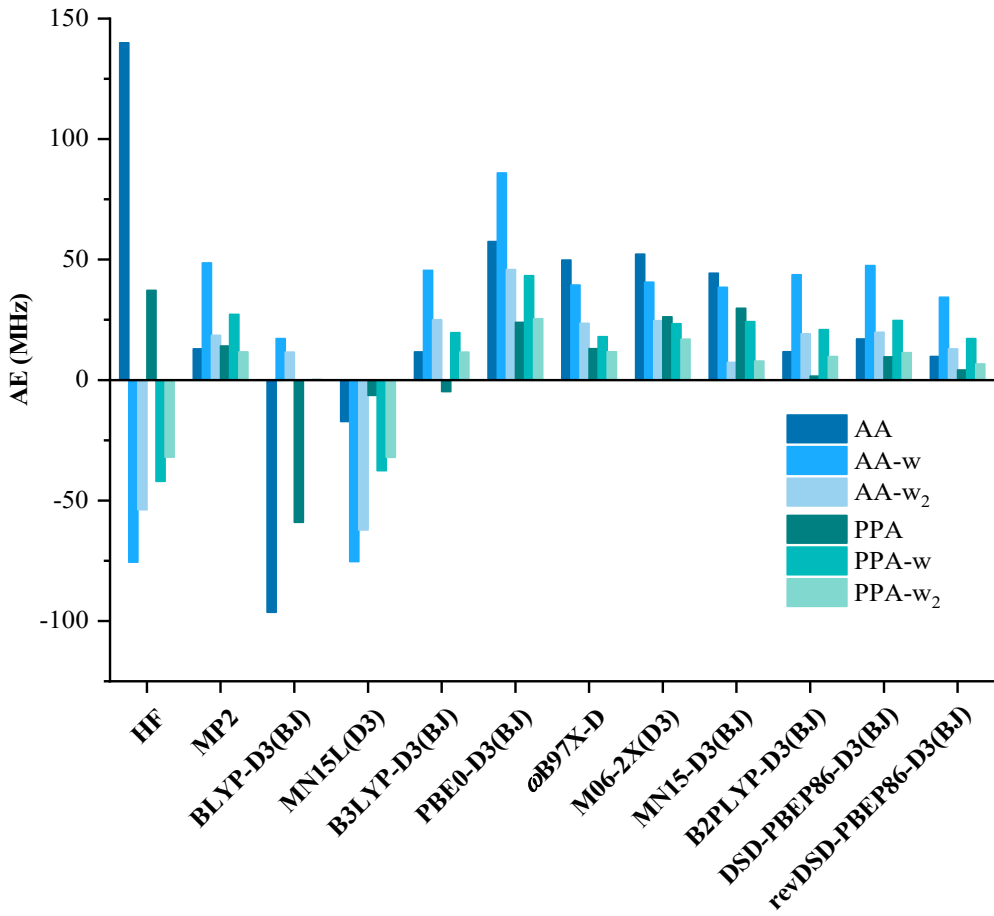


Table S3 Systematic error of calculating rotational constants with twelve different methods

	B2PLYP-D3(BJ)	B3LYP-D3(BJ)	BLYP-D3(BJ)	DSD-PBEP86-D3(BJ)	HF	M06-2X(D3)	MN15-D3(BJ)	MN15L(D3)	MP2	PBE0-D3(BJ)	revDSD-PBEP86-D3(BJ)	ωB97X-D
A(slope)	0.98984	0.99992	0.95905	0.99123	1.08079	1.00871	1.01366	1.02546	0.98709	0.99396	0.9926	1.00406
B(slope)	0.99925	0.99675	0.97996	0.99992	1.02424	1.00266	1.00173	1.00125	1.00257	1.00288	0.99922	1.00267
C(slope)	0.99818	0.99729	0.97492	0.99917	1.04408	1.0069	1.00759	1.00771	0.99833	1.00349	0.99903	1.0068
MAD	0.00424	0.00535	0.02869	0.00323	0.04970	0.00609	0.00766	0.01147	0.00572	0.00414	0.00305	0.00451
A(intercept)	108.40073	129.45978	207.90388	96.60279	-464.3187	22.18935	-43.40296	-340.1455	105.00327	171.91164	70.97013	71.37058
B(intercept)	27.94642	32.06445	38.12499	31.56615	-	107.8595	28.69889	24.0072	-58.44224	30.44168	52.36618	22.60308
C(intercept)	21.99836	24.34172	36.43542	23.5586	-	105.4792	14.85106	7.9139	-56.16142	26.0097	38.98884	16.38501
MAD	52.781837	61.955317	94.154763	50.575847	225.8858	21.9131	25.10802	151.58305	53.818217	87.755553	36.65274	33.430783
A(R^2)	0.99998	0.99998	0.99995	0.99999	0.99989	0.99995	0.99996	0.99997	0.99999	0.99999	0.99999	0.99998
B(R^2)	0.99996	0.99994	0.99991	0.99997	0.99979	0.99999	0.99998	0.99984	0.99997	0.9999	0.99998	0.99998
C(R^2)	0.99993	0.9999	0.99985	0.99993	0.99962	0.99998	0.99997	0.99981	0.99993	0.99982	0.99996	0.99996

All of the results can show strong linear correlation. We consider the slope that is closer to 1 and has smaller error as the main dominance, and the intercept close to 0 is the auxiliary reference.

5. SAPT analysis

Table S4 SAPT energy of electrostatics, exchange, induction, dispersion and total SAPT2+(3) δMP2 energy

Electronic energy (kcal/mol)	Electrostatics	Exchange	Induction	Dispersion	Total SAPT2+(3)δMP2
AA-w	-21.3	24.8	-8.0	-6.5	-10.7
AA-w ₂ (i)	-29.4	32.3	-13.4	-8.3	-18.8
AA-w ₂ (ii)	-23.7	27.0	-10.2	-7.1	-14.0
AA-w ₂ (iii)	-28.5	33.6	-13.6	-8.1	-16.6
PPA-w	-20.9	24.8	-7.9	-6.6	-10.6
PPA-w ₂ (i)	-29.2	32.1	-13.3	-8.3	-18.7
PPA-w ₂ (ii)	-23.7	26.9	-10.1	-7.1	-14.0
PPA-w ₂ (iii)	-28.3	33.3	-13.4	-8.1	-16.5
BA-w	-20.9	24.8	-7.9	-6.6	-10.6
BA-w ₂ (i)	-29.1	32.1	-13.2	-8.4	-18.7
BA-w ₂ (ii)	-23.7	26.9	-10.1	-7.1	-14.0
BA-w ₂ (iii)	-28.2	33.2	-13.3	-8.1	-16.4
PTA-w	-20.9	24.8	-7.9	-6.6	-10.6
PTA-w ₂ (i)	-29.1	32.1	-13.2	-8.4	-18.7
PTA-w ₂ (ii)	-23.7	27.0	-10.2	-7.1	-14.0
PTA-w ₂ (iii)	-28.2	33.2	-13.3	-8.1	-16.4
HXA-w	-20.9	24.8	-7.9	-6.6	-10.6
HXA-w ₂ (i)	-29.1	32.1	-13.2	-8.4	-18.7
HXA-w ₂ (ii)	-23.7	27.0	-10.2	-7.1	-14.0
HXA-w ₂ (iii)	-28.2	33.2	-13.3	-8.1	-16.4

Table S5 Energy (Thermo correction + electronic energy) of the substances under different temperature

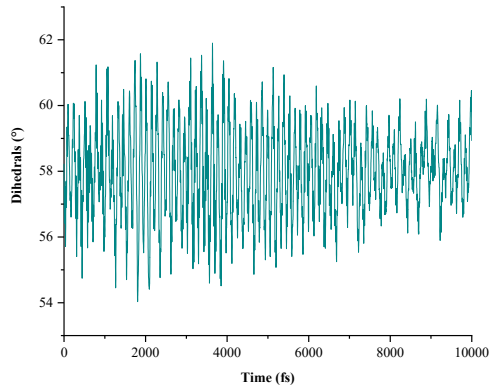
G(A.U.)	0	2 K	4 K	5 K	6 K	8 K	10 K	30 K	50 K	100 K	150 K	200 K	273K	298 K	350 K
AA	228.733	228.733	228.733	228.733	228.733	228.733	228.733	228.734	228.736	-228.74	228.745	228.749	228.757	-228.76	228.766
AA-w	305.068	305.068	305.068	305.068	305.068	305.068	305.069	-305.07	305.072	305.076	305.081	305.087	305.096	305.099	305.106
AA-w ₂	381.405	381.405	381.405	381.405	381.405	381.405	381.405	381.407	381.408	381.413	381.419	381.426	381.436	-381.44	381.449
PPA	267.952	267.952	267.952	267.952	267.953	267.953	267.953	267.954	267.956	-267.96	267.965	-267.97	267.979	267.982	267.988
PPA-w	344.288	344.288	344.288	344.288	344.288	344.288	344.288	-344.29	344.291	344.296	344.302	344.308	344.317	344.321	344.329
PPA-w ₂	420.624	420.624	420.624	420.624	420.625	420.625	420.625	420.626	420.628	420.633	-420.64	420.647	420.658	420.662	420.671
BA	307.172	307.172	307.172	307.172	307.172	307.172	307.172	307.174	307.175	-307.18	307.185	307.191	-307.2	307.203	307.211
BA-w	383.507	383.507	383.507	383.507	383.508	383.508	383.508	383.509	383.511	383.516	383.522	383.529	383.539	383.543	383.551
BA-w ₂	459.844	459.844	459.844	459.844	459.844	459.844	459.844	459.846	459.848	459.853	-459.86	459.867	459.879	459.884	459.893
PTA	346.392	346.392	346.392	346.392	346.392	346.392	346.392	346.394	346.395	-346.4	346.406	346.412	346.422	346.426	346.433
PTA-w	422.727	422.727	422.727	422.727	422.727	422.727	422.728	422.729	422.731	422.736	422.743	-422.75	422.761	422.765	422.774
PTA-w ₂	499.064	499.064	499.064	499.064	499.064	499.064	499.064	499.066	499.068	499.074	499.081	499.088	499.101	499.106	499.116
HXA	385.611	385.611	385.612	385.612	385.612	385.612	385.612	385.614	385.615	385.621	385.627	385.633	385.644	385.648	385.656
HXA-w	461.947	461.947	461.947	461.947	461.947	461.947	461.947	461.949	461.951	461.957	461.963	461.971	461.983	461.987	461.997
HXA-w ₂	538.283	538.283	538.284	538.284	538.284	538.284	538.284	538.286	538.288	538.294	538.301	538.309	538.323	538.328	538.339
H ₂ O	76.3229	76.3228	76.3229	76.3229	76.3229	-76.323	-76.323	76.3238	76.3247	76.3274	76.3304	76.3337	76.3387	76.3405	76.3443

Table S6 ΔG of the in the water-losing process at different tempertures

ΔG	0	2 K	4 K	5 K	6 K	8 K	10 K	30 K	50 K	100 K	150 K	200 K	273 K	298 K	350 K
AA-w	7.928	7.939	7.928	7.920	7.909	7.885	7.856	7.454	6.947	5.506	3.978	2.427	0.158	-0.615	-2.208
AA-w ₂	8.573	8.583	8.572	8.563	8.552	8.527	8.497	8.096	7.603	6.223	4.761	3.274	1.092	0.349	-1.185
PPA-w	7.890	7.900	7.888	7.879	7.868	7.843	7.813	7.400	6.885	5.434	3.899	2.343	0.066	-0.709	-2.308
PPA-w ₂	8.568	8.578	8.565	8.556	8.545	8.518	8.489	8.081	7.583	6.193	4.720	3.222	1.026	0.278	-1.266
BA-w	7.889	7.899	7.886	7.876	7.865	7.838	7.807	7.387	6.868	5.413	3.876	2.318	0.037	-0.739	-2.341
BA-w ₂	8.575	8.584	8.571	8.561	8.550	8.523	8.493	8.084	7.586	6.197	4.726	3.231	1.037	0.290	-1.251
PTA-w	7.909	7.917	7.904	7.894	7.883	7.855	7.825	7.404	6.887	5.439	3.911	2.362	0.095	-0.676	-2.268
PTA-w ₂	8.571	8.580	8.567	8.557	8.545	8.518	8.488	8.076	7.576	6.181	4.705	3.203	1.001	0.251	-1.296
HXA-w	7.912	7.920	7.906	7.896	7.884	7.857	7.825	7.403	6.886	5.440	3.913	2.365	0.100	-0.670	-2.261
HXA-w ₂	8.573	8.581	8.568	8.558	8.546	8.519	8.488	8.075	7.575	6.179	4.701	3.198	0.994	0.244	-1.305

6. AIMD simulations for dihedral angle of the terminal methyl

Fig S3.1 Change of dihedral angle of the methyl of HXA-w in 10 ps (5K)



The dihedral angle of the methyl of the most stable structure is 58.01° and it varies from 54.03° to 61.90° .

Fig S3.2 Change of dihedral angle of the methyl of BA-w in 10 ps (50K)

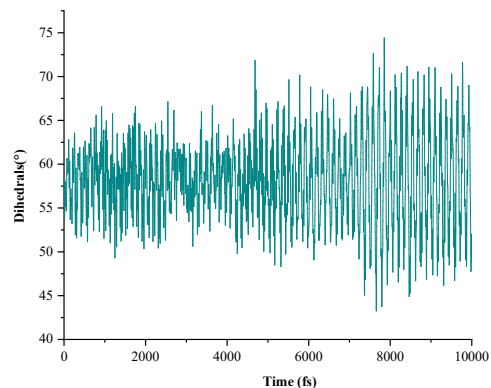


Fig S3.3 Change of dihedral angle of the methyl of BA-w in 10 ps (100K)

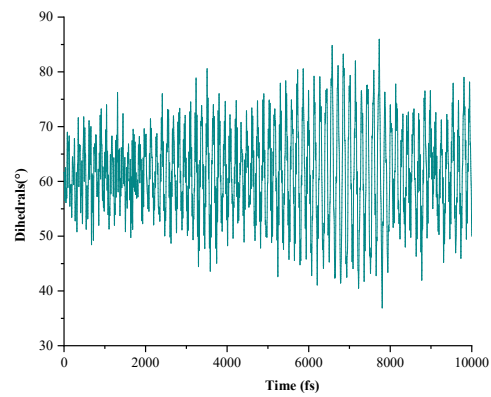


Fig S3.4 Change of dihedral angle of the methyl of HXA-w in 10 ps (50K)

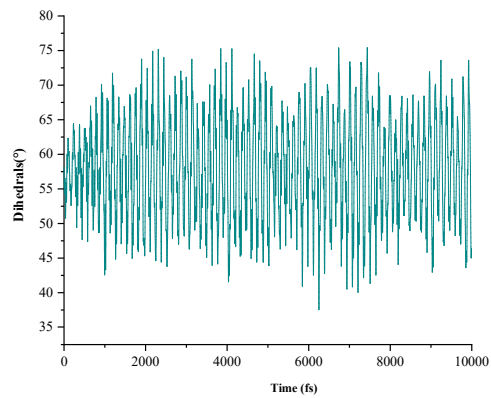


Fig S3.5 Change of dihedral angle of the methyl of HXA-w in 10 ps (100K)

